Metallointercalators: Syntheses, Structures, and Photochemical Characterizations of Phenanthrenequinone Diimine Complexes of Rhodium(III)

Achim H. Krotz,† Louis Y. Kuo,‡ and Jacqueline K. Barton*

Division of Chemistry and Chemical Engineering, California Institute of Technology, Pasadena, California 91125

Received June 22, 1993®

Short and very efficient syntheses of a series of d^6 rhodium(III) complexes, $[Rh(X_4)phi]^{3+}$ ($X_4 = (NH_3)_4$, $(en)_2$, tren, [12]aneN$_4$, [12]aneS$_4$), containing the 9,10-phenanthrenequinone diimine (phi) ligand and mono-, bi-, and tetradentate amine- or sulfur-containing ligands have been carried out. The synthetic strategies include two-step reaction sequences, in which the coordinated chlorides of $[Rh(X_4)Cl_2]^+$ are replaced by 9,10-diaminophenanthrene, and a single-step method, in which $RhCl_3$ is first reacted with 9,10-diaminophenanthrene and then the ancillary ligands are added, followed by oxidation with dioxygen. The complexes have been investigated with respect to their solid-state structure, spectroscopy, and photochemical reactivity. This detailed characterization provides the basis to explore systematically the contributions of hydrogen bonding and van der Waals interaction to sequence-specific recognition of DNA. Crystal structures of $[Rh[(NH_3)_4phi]Cl_3 \cdot 3H_2O$ (triclinic crystal system, space group $P\bar{1}$ (No. 2), $Z = 2$, $a = 7.605(2)$ Å, $b = 9.081(2)$ Å, $c = 16.729(4)$ Å, $\alpha = 87.95(2)°$, $\beta = 76.92(2)°$, $\gamma = 84.42(2)°$, $V = 1119.9(4)$ Å^3), $[Rh([12]aneN_4)phi](SCN)_3 \cdot 2H_2O$ (triclinic crystal system, space group $P\bar{1}$ (No. 2), $Z = 2$, $a = 15.479(5)$ Å, $b = 12.312(2)$ Å, $c = 8.679(2)$ Å, $\alpha = 72.10(2)°$, $\beta = 83.98(2)°$, $\gamma = 71.52(2)°$, $V = 1492.7(7)$ Å^3), and $Rh([12]aneS_4)phi]Br_3 \cdot 3H_2O$ (triclinic crystal system, space group $P\bar{1}$ (No. 2), $Z = 2$, $a = 8.921(2)$ Å, $b = 12.846(4)$ Å, $c = 13.325(4)$ Å, $\alpha = 70.50(2)°$, $\beta = 86.43(2)°$, $\gamma = 86.68(2)°$, $V = 1435.5(7)$ Å^3) are reported. Two isomers, which are also seen in solution in a ratio of 60:40 ($\Delta G = 0.99$ kJ/mol), of C_{2v} (14% population) and C_s (86% population) symmetry have been found in the same crystal of $[Rh([12]aneN_4)phi](SCN)_3 \cdot 2H_2O$, but only one isomer (point group C_s) has been found for the sulfur analogue $[Rh([12]aneS_4)phi]Br_3$. The substantial distortion of the octahedral geometry in the complexes $[Rh([12]aneN_4)phi]^{3+}$ and $[Rh([12]aneS_4)phi]^{3+}$ is associated with the small hole size of the coordinating macrocycles. Angles N(4)–Rh–N(6) between axial nitrogen atoms are as small as 160° in $[Rh([12]aneN_4)phi]^{3+}$ or 168.5° for the angle S(1)–Rh–S(3) between the axial sulfur atoms of $[Rh([12]aneS_4)phi]^{3+}$. The effect on the overall topology of different conformations of the independently coordinating bidentate ligands in $[Rh(en)_2phi]^{3+}$ is compared to the largely restricted conformations of tetradentate macrocycles in $[Rh([12]aneN_4)phi]^{3+}$ and $[Rh([12]aneS_4)phi]^{3+}$. ^{13}C and ^1H NMR spectroscopic data show that the structures seen in the solid state are also retained in solution. The chemical shift of the C1 or C8 hydrogen atom of the phi ligand is systematically influenced by the relative configuration at the heteroatom which is coordinated to the rhodium in the equatorial position. Electronic absorption spectra of the phi complexes of rhodium are found to be quite similar, dominated by strong bands between 250 and 280 nm and a broad transition between 360 and 410 nm. A reversible blue shift and hypochromicity (13–32%) are observed in the UV spectrum upon changing the pH from 2 to 10. The optical pK_a values for the phi complexes are correlated with the pK_b values of the ancillary ligands. $[Rh(X_4)phi]^{3+}$ complexes undergo photodecomposition upon irradiation with UV light at 325 nm with the preferential loss of the phi ligand. The pH dependence of the quantum yields for photoanation supports a mechanism in which light-induced charge transfer from the aromatic phi ligand to the rhodium(III) center is involved.

Introduction

Our laboratory has focused on the construction of transition metal complexes which bind DNA noncovalently with site selectivity in order to explore systematically those factors which contribute to DNA site recognition.[1,2] We have focused recently upon 9,10-phenanthrenequinone diimine (phi) complexes of rhodium(III), which bind DNA avidly by intercalation and, with photoactivation, promote DNA strand cleavage.[3,4] Two-dimensional NMR experiments of $[Rh(phen)_2phi]^{3+}$ bound to an oligonucleotide provide direct evidence for intercalation by the phi complex in the major groove of DNA.[5] Product analysis after photoinduced cleavage of oligonucleotides with $[Rh(phen)_2phi]^{3+}$ and $[Rh(phi)_2bpy]^{3+}$ yields results which are consistent with photoinduced cleavage being promoted through the direct abstraction of the C3′–hydrogen atom in duplex DNA by the intercalated phi ligand.[4] These octahedral complexes are useful in probing nucleic acid structure and recognition owing to the kinetic inertness of the d^6 rhodium(III) center, the relative rigidity of the complexes, their high binding affinity ($\log K \geq 6$) to nucleic acids through intercalation, and their rich photochemistry which permits methods to monitor sites of binding on the biopolymer with high resolution.

We have earlier reported different strategies for the synthesis of a series of phi complexes of rhodium(III) and ruthenium(II) with chelating aromatic ligands such as 2,2′-bipyridine and 1,10-phenanthroline, and we have described their photochemical properties.[6] These bulky complexes recognize nucleic acid sites

* Author to whom correspondence should be addressed.
† Present address: Research Center for Medical Biotechnology, Universitetsparken 5, DK-2100 Copenhagen 0, Denmark.
‡ Present Address: Department of Chemistry, Lewis and Clark College, Portland, OR 97219.
® Abstract published in *Advance ACS Abstracts*, November 15, 1993.
(1) Pyle, A. M.; Barton, J. K. *Prog. Inorg. Chem.* **1990**, *38*, 413.
(2) Sitlani, A.; Barton, J. K. *Handbook on Metal-Ligand Interaction in Biological Fluids*; Marcel Dekker: New York, in press.
(3) Pyle, A. M.; Long, E. C.; Barton, J. K. *J. Am. Chem. Soc.* **1989**, *111*, 4520.
(4) Sitlani, A.; Long, E. C.; Pyle, A. M.; Barton, J. K. *J. Am. Chem. Soc.* **1992**, *114*, 2303.
(5) David, S. S.; Barton, J. K. *J. Am. Chem. Soc.* **1993**, *115*, 2984.
(6) Pyle, A. M.; Chiang, M.; Barton, J. K. *Inorg. Chem.* **1990**, *29*, 4487.

0020-1669/93/1332-5963$04.00/0

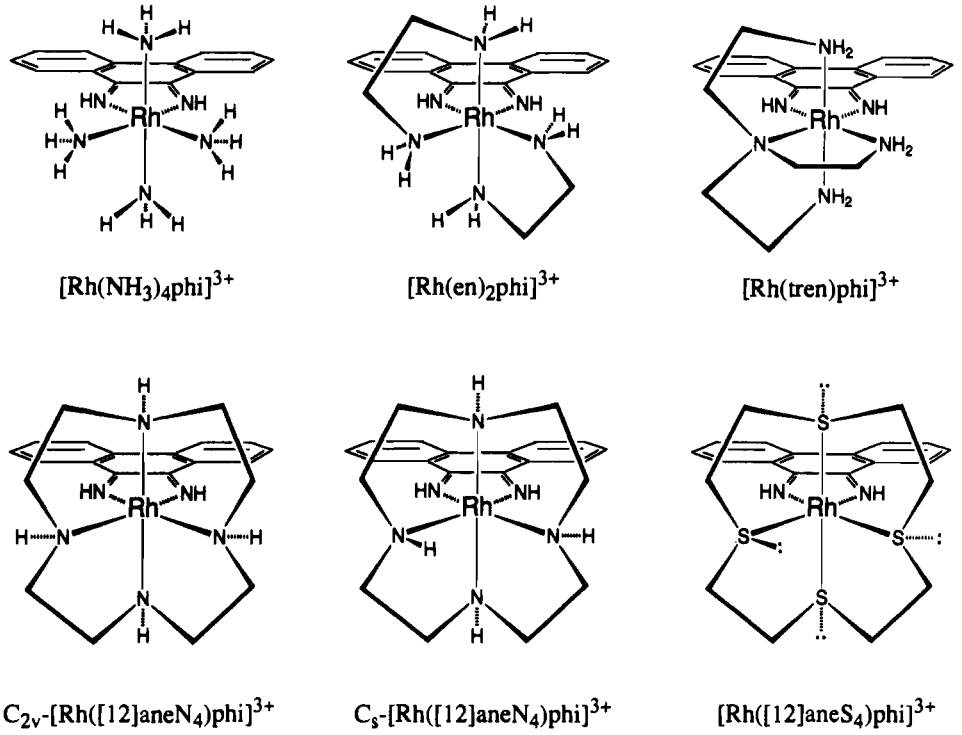

Figure 1. Schematic illustration of different phi complexes of rhodium(III).

primarily through *shape-selection*.[1,7,8] For example, with $[Rh(phen)_2phi]^{3+}$, because of the steric constraints of the overhanging phenanthroline ligands, intercalation is available only at sites on duplex DNA, where the major groove is somewhat opened through the propeller twisting of the DNA base pairs.[7] As a result of comparable steric considerations, $[Rh(phen)_2phi]^{3+}$ also serves as a novel probe for sites of tertiary interaction in folded RNA molecules.[9]

Phi complexes of rhodium now appear to offer a general strategy to examine DNA recognition through the construction of a series of intercalating phi complexes with variable functionalities in the ancillary positions and the systematic examination of their recognition characteristics. Recently we reported the results of DNA recognition studies for a series of phi complexes of Rh(III), $[Rh(X)_4phi]^{3+}$ $[(X)_4 = (NH_3)_4, (en)_2, [12]aneN_4, [12]aneS_4$; en = ethylenediamine; $[12]aneN_4$ = 1,4,7,10-tetraazacyclododecane; $[12]aneS_4$ = 1,4,7,10-tetrathiacyclododecane], with aliphatic mono-, bi-, and tetradentate amines and a macrocyclic thioether as ancillary ligands (Figure 1).[10] These complexes also bind avidly to DNA through intercalation and, with photoactivation, promote strand cleavage. Moreover, in contrast to complexes containing phenanthrolines in the ancillary positions $[Rh(NH_3)_4phi]^{3+}$, $[Rh(en)_2phi]^{3+}$, $[Rh([12]aneN_4)phi]^{3+}$, and $[Rh([12]aneS_4)phi]^{3+}$ exhibit DNA recognition characteristics which are based primarily on their ability to form hydrogen bonds and specific van der Waals contacts with the functional groups of the DNA bases located in the major groove. Indeed, using this same strategy, by elaboration of the ancillary ligands of a phi complex to present methyl groups and hydrogen-bonding donors to the DNA helix in defined positions in three-dimensional space, the complex Δ,α-[Rh[(2*R*,9*R*)-2,9-diamino-4,7-diazadecane]phi]$^{3+}$ was designed specifically to bind to the sequence 5′-TGCA-3′.[11] Thus, phi complexes of rhodium(III) offer a route to the *predictive* design of sequence-specific DNA binding agents.

For the rational construction of novel rhodium complexes with DNA sequence-specificity, what is, therefore, required is high-resolution information concerning their three-dimensional structures and an understanding of their spectroscopy and photoreactivity. In this report we describe new, efficient strategies for the preparation of the complexes $[Rh(NH_3)_4phi]Cl_3$, $[Rh(en)_2phi]Cl_3$, $[Rh(tren)phi](ClO_4)_3$ (tren = tris(2-aminoethyl)amine), $[Rh([12]aneN_4)phi]Cl_3$, and $[Rh([12]aneS_4)phi]Cl_3$. The structures in solution have been characterized by ^1H and ^{13}C NMR and UV–visible spectroscopy. X-ray crystallographic studies of $[Rh(NH_3)_4phi]^{3+}$, $[Rh([12]aneN_4)phi]^{3+}$, and $[Rh([12]aneS_4)phi]^{3+}$ provide the requisite information concerning the structures of the complexes to atomic detail. The differences in shape caused by ring puckering of the chelating ligands, by the strain of a metal-coordinated macrocycle, and by different bond lengths are discussed. The photophysical and photochemical properties of these complexes are also described as a function of pH.

Experimental Section

Materials. 9,10-Diaminophenanthrene (DAP), ethylenediamine, tren, 1,4,7,10-tetraazacyclododecane ($[12]aneN_4$), and 1,4,7,10-tetrathiacyclododecane ($[12]aneS_4$) were purchased from Aldrich and were used without further purification. $RhCl_3$ was purchased from Aesar, Johnson-Matthey, and Aldrich. Trifluoroacetic acid (TFA) was purchased from EM Science. The complexes *cis*-$[Rh(NH_3)_4Cl_2]Cl$, $[Rh(en)_2Cl_2]Cl$, $[Rh(tren)Cl_2]Cl$, $[Rh([12]aneN_4)Cl_2]Cl$, and $[Rh([12]aneS_4]Cl_2]Cl$ were synthesized according to published procedures.[12-16]

Instrumentation. Fourier-transformed ^1H NMR spectra were taken with a JEOL GX-400 spectrometer at 400 MHz or with a General Electric QE-300 spectrometer in D_2O (referenced to 4.65 ppm) or d_6-DMSO (referenced to 2.49 ppm). ^{13}C NMR spectra were recorded with a General Electric spectrometer at 75 MHz with full proton decoupling. UV/visible spectra were recorded on a Cary 2200 spectrophotometer. A Liconix helium/cadmium laser (Model 4240) was used for irradiations at 325 nm. High-performance liquid chromatography (HPLC) was

(7) Pyle, A. M.; Morii, T.; Barton, J. K. *J. Am. Chem. Soc.* **1990**, *112*, 9432.
(8) Uchida, K.; Pyle, A. M.; Morii, T.; Barton, J. K. *Nucleic Acids Res.* **1989**, *17*, 10259.
(9) Chow, C. S.; Behlen, L. S.; Uhlenbeck, O. C.; Barton, J. K. *Biochemistry* **1992**, *31*, 972.
(10) Krotz, A. H.; Kuo, L. Y.; Shields, T. P.; Barton, J. K. *J. Am. Chem. Soc.* **1993**, *115*, 3877.
(11) Krotz, A. H.; Hudson, B. P.; Barton, J. K. Submitted for publication.
(12) (a) Addison, A. W. *J. Chem. Soc., Dalton Trans.* **1972**, 589. (b) Hancock, M. P. *Acta Chem. Scand.* **1975**, *A29*, 468.
(13) Dixon, N. E.; Lawrance, G. A.; Lay, P. A.; Sargeson, A. M. *Inorg. Chem.* **1984**, *23*, 2940.
(14) Martins, E.; Sheridan, P. S. *Inorg. Ch em.* **1978**, *17* (10), 2822.
(15) Collman, J. P.; Schneider, P. W. *Inorg. Chem.* **1966**, *5* (8), 1380.
(16) Blake, A. J.; Reid, G.; Schröder, M. *J. Chem. Soc., Dalton Trans.* **1985**, 1675.

carried out using a Waters 600/600E multisolvent delivery system equipped with a Waters 484 tunable absorbance detector and a VYDAC protein and peptide C_{18} column.

Measurement of pH-Dependent Optical Changes. An aqueous solution of the rhodium complex (50 μM) in water (40 mL) was brought to pH 2 by addition of HCl. The solution was stirred vigorously, and the pH was monitored with a pH meter. After addition of aliquots of 1, 0.1, or 0.01 N aqueous NaOH to the solution, the pH was recorded and 1 mL was withdrawn for recording the UV/vis spectrum. After scanning, the solution was returned to the remaining 39 mL of solution and the cycle was repeated in order to monitor spectral changes at pH intervals of approximately 0.3 pH units up to pH 11. In order to ensure that the changes were reversible, the pH was then lowered to the starting pH and the spectra were compared.

Ferrioxalate Actinometry. Ferrioxalate actinometry[17] was used to calibrate the photon flux from the He/Cd laser. Photon flux was calibrated before every photolysis experiment, by using three trials and a control at the irradiation wavelength of 325 nm. With our irradiation geometry, the photon flux values for the experiments described fell within the range (1.25–2.08) × 10^{-6} Einstein/min.

Photolysis of Rhodium(III) Complexes and Determination of Quantum Yields. Solutions of $[Rh(NH_3)_4phi]^{3+}$, $[Rh(en)_2phi]^{3+}$, $Rh([12]aneN_4)phi]^{3+}$, $[Rh(phen)_2phi]^{3+}$, and $[Rh([12]aneS_4)phi]^{3+}$ (5 mL, 30–70 μM) in buffer R (50 mM NaCl, 5 mM Tris, pH 7) were added to a quartz cuvette (l = 2 cm, V = 5 cm^3) containing a small stir bar. If the experiment was performed at a different pH, the pH was adjusted to 10 by adding NaOH or to 2 by adding HCl. The cuvette was positioned in the beam of the He/Cd laser and irradiated for time intervals of 5–15 min, if the experiment was performed at a pH higher than the pK_a of the complex, or at intervals of several hours, if the pH of the solution was lower than the pK_a of the complex, while the solution was stirred vigorously. The electronic absorption spectrum of the solution was recorded after each time interval. Care was taken to obtain an array of readings at short irradiation times where the reaction was less than 30% complete and the plot of absorption versus time was linear. The extent of photoreaction with time was quantitated on the basis of absorbance changes at 373 nm for $[Rh(NH_3)_4phi]^{3+}$, at 375 nm for $[Rh(en)_2phi]^{3+}$, at 378 nm (pH 11) and at 395 nm (pH 7) for $[Rh([12]aneN_4)phi]^{3+}$, at 362 nm (pH 7) and a 378 nm (pH 2) for $[Rh(phen)_2phi]^{3+}$, and at 364 nm (pH 7) and at 383 nm (pH 2) nm for $[Rh([12]aneS_4)phi]^{3+}$. The photoproducts did not absorb to a substantial amount at the monitoring wavelength. In the determination of quantum yields for the photoreaction only initial irradiation time points were used.

Warning! *The perchlorate salts prepared in this work are potentially explosive and must be handeled with great care.* Only small amounts should be prepared. However, we have not experienced any problems with the complexes described in this work.

(Tris(2-aminoethyl)amine)(9,10-phenanthrenequinone diimine)rhodium(III) Triperchlorate, [Rh(tren)phi](ClO$_4$)$_3$. A solution of $[Rh(tren)Cl_2]Cl$ (35 mg, 0.1 mmol) in 0.1 N aqueous NaOH was refluxed for 30 min. After cooling to room temperature, the light yellow solution was degassed and neutralized to pH 7 by dropwise addition of 0.5 M $HClO_4$. This solution was added via syringe to a dioxygen-free suspension of 9,10-diaminophenanthrene (100 mg, 0.48 mmol) in 5 mL of ethanol. After reflux of the reaction mixture for 3 h, it was filtered and allowed to cool to room temperature. The dark red suspension was exposed to air overnight, followed by repeated filtration. After replacement of the sovlent with water, the Rh complex was precipitated by dropwise addition of an aqueous $NaClO_4$ solution. ^{1}H NMR (400 MHz, D_2O): δ (ppm) 8.5 (d, 1H), 8.1 (d, 3H), 7.7 (2t, 2H), 7.5 (2t, 2H), 4.1 (m, 2H), 3.1–3.4 (m, 10H). UV/vis [nm ($10^{-3}\epsilon$, M^{-1} cm^{-1})]: 252 (17.7), 263 (sh, 21.5), 271 (24.3), 285 (sh, 10.9), 371 (12.7), 390 (sh, 11.4). Anal. Calcd for $[Rh(tren)phi]Cl_3 \cdot 3H_2O$ (fw 615.79): C, 39.01; H, 5.56; N, 13.65. Found: C, 39.08; H, 5.04; N, 13.09. FAB/MS(+) of $[Rh(tren)phi](ClO_4)_3$ (m/z, assignment): 553, $[Rh(tren)phi(ClO_4)]^+$; 453, $[Rh(tren)phi]^+$.

Bis(ethylenediamine)(9,10-phenanthrenequinone diimine)rhodium(III) Trichloride, [Rh(en)$_2$phi]Cl$_3$. Under exclusion of air (N_2 atmosphere), a suspension of $RhCl_3$ (100 mg, 0.44 mmol) and 9,10-diaminophenanthrene (94 mg, 0.45 mmol) in 3 mL of water was refluxed for 1 h. After cooling of the suspension to room temperature, 15 mL of degassed DMF was added and the reaction mixture was heated to 120 °C for 5 min. After cooling of the mixture to about 50 °C, a solution of ethylenediamine (106 mg, 0.88 mmol) in 5 mL of degassed DMF was added via syringe to the reaction mixture and heated to 120 °C for 10 min to form a deep red solution. After cooling to room temperature, this solution was added to 100 mL of water/ethanol (75:25) and was stirred under exposure to air for several hours. The reaction mixture was filtered and loaded on a cation-exchange column (Sephadex SP C50) (eluent: 0.1 N HCl and then 0.5 N HCl). An orange band was eluted, and fractions showing the characteristic UV absorption at 376 nm were combined. The solvent volume was reduced to 2 mL, and the red crystals were filtered. Yield: 130 mg (55%) of $[Rh(en)_2phi]Cl_3 \cdot 3H_2O$. Spectroscopic data were identical to those reported previously.[10]

(9,10-Phenanthrenequinone diimine)(1,4,7,10-tetraazacyclododecane)rhodium(III) Trichloride, [Rh([12]aneN$_4$)phi]Cl$_3$. Under exclusion of air (N_2 atmosphere) a solution of $[Rh([12]aneN_4)Cl_2]Cl$ (300 mg, 0.72 mmol) in 10 mL of 0.2 M aqueous NaOH was refluxed for 30 min. After cooling of the solution to room temperature, the pH was brought to 6.5 by dropwise addition of 0.5 M $HClO_4$. This solution was added to a degassed suspension of 9,10-diaminophenanthrene (180 mg, 0.87 mmol), 1 g of $NaClO_4$, and 6 mL of ethanol. The reaction mixture was refluxed for 5 h, and after cooling to room temperature, it was allowed to oxidize in air for 2 days. The mixture was filtered and the residue was extracted several times with water. The filtrates were combined and purified by cation-exchange chromatography (Sephadex-SP C50) (eluent: 0.05 N HCl and then 0.3 N HCl). Fractions showing the UV absorption at 395 nm were combined and evaporated to dryness, yield 200 mg (47%). HPLC analysis (C_{18}, λ = 254 nm, acetonitrile/H_2O/TFA = 10:90:0.1, f = 5.5 mL/min, t_{R0} = 2.2 min) showed two baseline resolved peaks at t_R = 14 min (40%) for C_s-$[Rh([12]aneN_4)phi]^{3+}$ and 16 min (60%) for C_{2v}-$[Rh([12]aneN_4)phi]^{3+}$. ^{1}H NMR (two isomers, 300 MHz, D_2O): δ (ppm) 8.47 (d, <1H), 8.15 (m, ~7H), 7.7 (t, 4H), 7.5 (t, 4H), 2.95–3.6 (m, 32H). ^{13}C NMR (two isomers, 75.47 MHz, D_2O): δ (ppm) 174.4, 174.0, 173.5*, 137.1, 136.9*, 134.3, 134.0*, 133.8, 130.5*, 130.3, 128.3, 127.4*, 126.0*, 125.5, 125.0, 124.9*, 60.6*, 59.9, 55.9, 52.6, 51.8*, 48.4, 51.8 (an asterisk denotes signals assigned to the C_{2v}-symmetric isomer). UV/vis [nm (10^{-3} ϵ, M^{-1} cm^{-1})]: at pH 7, 252 (27.3), 263 (26.6), 271 (28.8), 287 (sh, 12.9), 395 (16.7), 410 (sh, 15.2); isosbestic point, 359 (9.1). FAB/MS (m/z (%, assignment)): 551 (10, $[[Rh([12]aneN_4)phi]Cl_2]^+$), 515 (29, $[[Rh([12]aneN_4)phi]Cl - H]^+$), 480 (72, $[[Rh([12]aneN_4)phi] - H]^+$), 309 (20, $[Rhphi]^+$), 273 (74, $[Rh([12]aneN_4) - 2H]^+$). Anal. Calcd for $[Rh([12]aneN_4)phi](SCN)_3 \cdot 2H_2O$ (fw 681.7): C, 44.57; H, 4.79; N, 18.71. Found: C, 44.71; H, 4.49; N, 18.32.

(9,10-Phenanthrenequinone diimine)(tetraammine)rhodium(III) Trichloride Trihydrate, [Rh(NH$_3$)$_4$phi]Cl$_3$·3H$_2$O. Under exclusion of air (N_2 atmosphere) a mixture of $RhCl_3$ hydrate (500 mg, 2.2 mmol) and 9,10-diaminophenanthrene (500 mg, 2.4 mmol) in 10 mL of H_2O was refluxed for 1 h to form a yellow precipitate. The suspension was frozen with liquid nitrogen, 5 mL of NH_4OH was added, and the mixture was degassed. The reaction mixture was refluxed for 45 min. A blue-black precipitate formed. After cooling of the mixture to room temperature, 100 mL of H_2O was added. After filtration the filtrate was exposed to air overnight and purified by cation-exchange chromatography (Sephadex-SP C50) (eluent: 0.1 N HCl and then 0.2 N HCl). An orange band giving the characteristic UV absorption at λ = 372 nm was collected and evaporated to dryness. Yield: 700 mg (59%). ^{1}H NMR (300 MHz, D_2O): δ 8.22 (d, J = 8 Hz, 2H), 8.14 (d, J = 8 Hz, 2H), 7.66 (t, J = 8 Hz, 2H), 7.48 (t, J = 8 Hz, 2H) ppm. ^{1}H NMR (300 MHz, d_6-DMSO): δ (ppm) 14.2 (s (br), 2H, imine H), 8.73 (d, J = 8 Hz, 2H), 8.48 (d, J = 8 Hz, 2H), 7.84 (t, J = 8 Hz, 2H), 7.70 (t, J = 8 Hz, 2H), 4.6 (s, 6H, $2NH_3$), 3.75 (s, 6H, $2NH_3$). ^{13}C NMR (75.47 MHz, D_2O): δ (ppm) 174.2, 136.4, 133.6, 130.0, 127.1, 125.0, 124.3. UV/vis [nm ($10^{-3}\epsilon$, M^{-1} cm^{-1})]: at pH 7, 252 (16.3), 263 (sh, 20.5), 270 (24.6), 283 (sh, 10.5), 372 (11.7), 386 (sh, 10.4); isosbestic points, 268 (23.5), 333 (4.2). Anal. Calcd for $[Rh(NH_3)_4phi]Cl_3 \cdot 3H_2O$ (fw 537.7): C, 31.27; H, 5.25; N, 15.63. Found: C, 30.72; H, 4.88; N, 15.52.

(9,10-Phenanthrenequinone diimine)(1,4,7,10-tetrathiacyclododecane)rhodium(III) Trichloride, [Rh([12]aneS$_4$)phi]Cl$_3$. Under exclusion of air (N_2 atmosphere), a mixture of $[Rh([12]aneS_4)Cl_2]Cl$ (450 mg, 1.0 mmol) and 9,10-diaminophenanthrene (230 mg, 1.1 mmol) in 60 mL of ethanol/water (1:1) was refluxed for 25 min. After cooling of the mixture to room temperature, 200 mL of water was added and the solution was exposed to air for 2 days. The solution was purified by cation-exchange chromatography (Sephadex SP C-50) (eluent: 0.1 N HCl and then 0.4 N HCl). A red band, showing the characteristic UV absorption was collected and evaporated to dryness, yielding 500 mg (71%). The dark purple solid was recrystallized in 5 mL of water at 4 °C. Yield: 400 mg. The mother liquor was diluted with 40 mL of water, and an aqueous

(17) Calvert, J. G.; Pitts, J. N. *Photochemistry*; John Wiley and Sons: New York, 1967.

Table I. Crystallographic Data and Details of Data Collection of Phi Complexes of Rhodium(III)

	compound		
	$[Rh(NH_3)_4phi]Cl_3 \cdot 3H_2O$	$[Rh([12]aneS_4)phi]Br_3 \cdot 3H_2O$	$[Rh([12]aneN_4)phi](SCN)_3 \cdot 2H_2O$
chem formula	$C_{14}H_{28}Cl_3N_6O_3Rh$	$C_{22}H_{32}Br_3N_2O_3S_4Rh$	$C_{25}H_{34}N_9O_2S_3Rh$
fw	537.68	843.38	691.71
color, habit	red, prismatic	red-brown plate	red skewed parallelepiped
space group	$P\bar{1}$ (No. 2)	$P\bar{1}$ (No. 2)	$P\bar{1}$ (No. 2)
cryst system	triclinic	triclinic	triclinic
a, Å	7.605(2)	8.921(2)	15.479(5)
b, Å	9.081(2)	12.846(4)	12.312(2)
c, Å	16.729(4)	13.325(4)	8.679(2)
α, deg	87.95(2)	70.50(2)	72.10(2)
β, deg	76.92(2)	86.43(2)	83.98(2)
γ, deg	84.42(2)	86.68(2)	71.52(2)
V, Å^3	1119.9(4)	1435.5(7)	1492.7(7)
Z	2	2	2
d_x, g cm^{-3}	1.59	1.98	1.54
cryst size, mm	0.12 × 0.22 × 0.56	0.02 × 0.11 × 0.26	0.10 × 0.24 × 0.30
μ, cm^{-1}	11.36	50.59	8.04
diffractometer	Enraf-Nonius Cad-4	Enraf-Nonius Cad-4	Enraf-Nonius Cad-4
radiation (λ, Å)	Mo Kα (0.710 73)	Mo Kα (0.710 73)	Mo Kα (0.710 73)
orientation reflcns	25	25	25
range (2θ), deg	$22 < 2\theta < 26$	$16 < 2\theta < 20$	$18 < 2\theta < 21$
temp, K	296	297	297
scan method	ω-scans	ω-scans	ω-scans
data collcn range (2θ), deg	$2 < 2\theta < 50$	$2 < 2\theta < 40$	$2 < 2\theta < 35$

NaBr solution was added to precipitate out the bromide salt. HPLC (C_{18}, λ = 254 nm, acetonitrile/H_2O/TFA = 12:88:0.1, f = 4.5 mL/min, t_{R0} = 2.5 min): t_R = 12.8 min. ^{1}H NMR (300 MHz, D_2O): δ 8.54 (d, J = 8 Hz, 1H), 8.21 (d, J = 8 Hz, 1H), 8.06 (2d, 2H), 7.65 (2t, 2H), 7.49 (2t, 2H), 3.44–4.25 (m, 16H) ppm. ^{13}C NMR (75.47 MHz, D_2O): δ (ppm) 175.2, 174.1, 137.1, 136.7, 134.4, 133.8, 129.9, 129.8, 128.5, 127.7, 125.2, 125.1, 125.0, 124.8, 45.0, 41.8, 38.0, 35.7. UV/vis [nm ($10^{-3}\epsilon$, M^{-1} cm^{-1})]: at pH 7, 252 (30.8), 261 (sh, 35.5), 268 (39.3), 283 (sh, 20.8), 331 (sh, 11.4), 359 (15.3); isosbestic points, 288 (15.3), 306 (7.0), 364 (15.0). FAB/MS of $[Rh([12]aneS_4)phi]Cl_3$ (fw 655.98) [m/z (%, assignment)]: 655 (2, $[[Rh([12]aneS_4)phi]Cl_3]^+$), 549 (5, $[Rh([12]aneS_4)phi]^+$), 343 (8, $[Rh[12]aneS_4]^+$). Anal. Calcd for $[Rh([12]aneS_4)phi]Cl_3 \cdot 3H_2O$ (fw 710.03): C, 37.22; H, 4.54; N, 3.95. Found: C, 36.55; H, 4.34; N, 3.94. Anal. Calcd for $[Rh([12]aneS_4)phi]Br_3 \cdot 3H_2O$: C, 31.33; H, 3.82; N, 3.32. Found: C, 31.07; H, 3.57; N, 3.43.

***N,N*-Bis(trimethylsilyl)phenanthrenequinone diimine (SiPHI).** This air- and water-sensitive, orange-colored compound was synthesized according to a published procedure.[18] Benzene was replaced by toluene, and crude SiPHI was recrystallized at −70 °C from dry toluene. ^{1}H NMR (300 MHz, d_6-benzene): δ (ppm) 0.34 (s, 18H), 6.96 (dd, 2H), 7.06 (dd, 2H), 7.44 (d, J = 7.9 Hz, 2H), 7.80 (d, J = 7.8 Hz, 2H). UV/vis [nm ($10^{-3}\epsilon$, M^{-1} cm^{-1})]: 253 (16.1), 260 (18.5), 265 (19.8), 300 (4.0), 360 (1.7).

Phenanthrenequinone diimine (phi). This water-sensitive compound was obtained according ref 18 by dissolving SiPHI in absolute ethanol. UV/vis [nm ($10^{-3}\epsilon$, M^{-1} cm^{-1})]: 253 (13.1), 260 (17.2), 265 (21.0), 300 (2.8), 367 (1.5).

Structural Determination of $[Rh(NH_3)_4phi]Cl_3 \cdot 3H_2O$. A red prismatic crystal was obtained from an aqueous solution of $[Rh(NH_3)_4phi]Cl_3$ by evaporation at room temperature. A total of 25 reflections with $22° < 2\theta < 26°$ were used to determine the cell dimensions. The crystal data are summarized in Table I. An analytical absorption correction was applied to the data set. The maximum and minimum transmission factors were 0.878 and 0.771, respectively. Data were collected from h = −9 to 9, k = −10 to 10, and l = −19 to 19. Three standard reflections (every 2.5 h) showed a decay of 0.6% during data collection. A total of 7928 reflections were measured; 3928 were independent and 3927 reflections were used in the refinement. The goodness of fit for merging was 0.963. Rhodium atom coordinates were found from the Patterson map, and remaining heavy atoms by successive structure factor-Fourier cycles. R = 0.028 on F for 3840 reflections with $F_o^2 > 0$, R = 0.025 on F for 3539 reflections with $F_o^2 > 3\sigma(F_o^2)$, and R_w = 0.005 on F^2 for 3927 reflections. Goodness of fit (S) = 2.27 for 3927 data and 245 parameters. $(\Delta/\sigma)_{max}$ in the final least-squares cycle <0.01. $\Delta\rho_{max}$ = +0.56 e Å^{-3} and $\Delta\rho_{min}$ = −0.53 e Å^{-3} in the final difference map. The secondary extinction parameter was 0.67(8) × 10^{-6}.[19] Scattering factors and f' and f'' were taken from ref 20a,b.

Structural Determination of $[Rh([12]aneS_4)phi]Br_3 \cdot 3H_2O$. A small red-brown plate was obtained from an aqueous solution of $[Rh([12]aneS_4)phi]Cl_3$ and NaBr by slow evaporation at room temperature. A total of 25 reflections with $16° < 2\theta < 20°$ were used to determine the cell dimensions. The crystal data are summarized in Table I. An analytical absorption correction was applied to the data set using the program CRYRM.[21] The maximum and minimum transmission factors were 0.98 and 0.90, respectively. Data were collected from h = −8 to 8, k = −12 to 12, and l = −12 to 12. Three standard reflections (every 2.5 h) showed a decay of 1.2% in 67 h of data collection. A total of 5448 reflections were measured; 2682 were independent, and 2681 reflections were used in the refinement. The goodness of fit for merging was 0.96. Multan 88[22] gave coordinates for Rh, three Br$^-$ ions and four S atoms, and the remaining heavy atoms were found after the structure factor-Fourier cycle. R = 0.046 on F for 2524 reflections with $F_o^2 > 0$, R = 0.038 on F for 2180 reflections with $F_o^2 > 3\sigma(F_o^2)$, and R_w = 0.008 on F^2 for 2681 reflections. Goodness of fit (S) = 2.29 for 2681 data and 316 parameters. $(\Delta/\sigma)_{max}$ in the final least-squares cycle < 0.01; $\Delta\rho_{max}$ = 1.11 e Å^{-3} and $\Delta\rho_{min}$ = −1.04 e Å^{-3} in the final difference map. The secondary extinction parameter was refined to 0 and left out of the final cycle.

Structural Determination of $[Rh([12]aneN_4]phi](SCN)_3 \cdot 2H_2O$. A red skewed parallelepiped was obtained from an aqueous solution of $[Rh([12]aneN_4]phi]Cl_3$ and KSCN by slow evaporation at room temperature. A total of 25 reflections with $18° < 2\theta < 21°$ were used to determine the cell dimensions. The crystal data are summarized in Table I. An empirical absorption correction was applied to the data set. The maximum and minimum transmission factors were 1.000 and 0.832, respectively. Data were collected from h = −13 to 13, k = −10 to 10, and l = −7 to 7. Three standard reflections (every 2.5 h) showed a decay of approximately 1%. A total of 7032 reflections were measured; 2784 were independent, and 2784 were used in the refinement. The goodness of fit for merging was 1.12. Rhodium atom coordinates were found from the Patterson map; the remaining heavy atoms were found by successive structure

(18) Tuchtenhagen, G.; Rühlmann, K. *Liebigs Ann. Chem.* **1968**, *711*, 174.

(19) Larson, A. C. *Acta Crystallogr.* **1967**, *23*, 644.

(20) (a) Cromer, D. T. *International Tables for X-ray Crystallography*; Kynoch Press: Birmingham, U.K., 1974; Vol. 4, pp 149–151 (present distributor Kluwer Academic Publishers, Dodrecht, The Netherlands). (b) Cromer, D. T., Waber, J. T. *International Tables for X-ray Crystallography*; Kynoch Press: Birmingham, U. K., 1974; Vol. 4, pp 99–101 (present distributor Kluwer Academic Publishers, Dordrecht, The Netherlands).

(21) Duchamp, D. J. *Am. Crystallogr. Assoc. Meet.*; Bozeman, MT, 1967; paper B-14, p 29.

(22) Debaerdemaeker, T.; Germain, G.; Main, P.; Refaat, L. S.; Tate, C.; Woolfson, M. M. Computer Programs for Automatic Solution of Crystal Structures from X-ray Diffraction Data. Univs of York, England, and Louvain, Belgium, 1988.

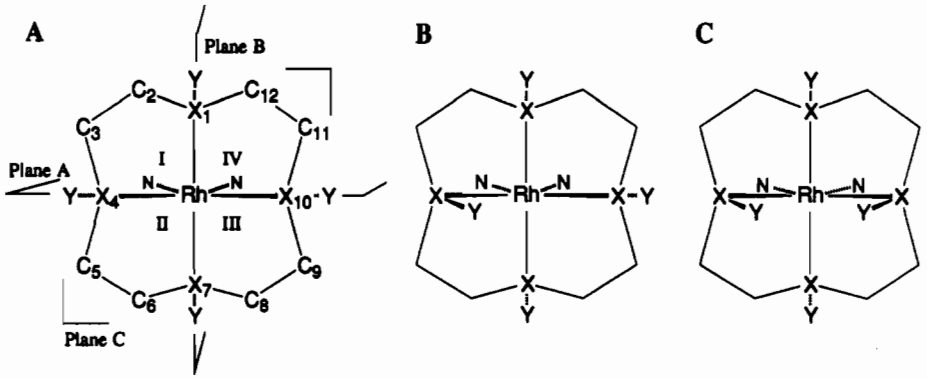

Figure 2. Three configurations of complexes with coordinated tetradentate macrocycles [12]aneN$_4$ or [12]aneS$_4$ with the numbering system: (A) all-exo; (B) exo, endo, exo, exo; (C) exo, endo, exo, endo.

factor-Fourier calculations. $R = 0.049$ on F for 2642 reflections with $F_o^2 > 0$, $R = 0.042$ on F for 2350 reflections with $F_o^2 > 3\sigma(F_o^2)$, and $R_w = 0.011$ on F^2 for 2784 reflections. Goodness of fit (S) = 2.49 for 2784 data and 343 parameters. $(\Delta/\sigma)_{max}$ in final least-squares cycle = 0.06; $\Delta\rho_{max} = 0.78$ e Å^{-3} and $\Delta\rho_{min} = -0.57$ e Å^{-3} in the final difference map.

The compound shows disorder in the tetraazacyclododecane ligand [near N(3)] and in the thiocyanate ions of S(3) and S(4). The configuration at N(3) as shown in Figure 5A has a population of 0.84(1); the compound with the inverted configuration at N(3), shown in Figure 5B, has a population of 1 – 0.84. This inversion gives a second HN(3), new C(15b) and C(22b) atoms with hydrogen atoms H(15C), H(15D), H(22C), and H(22D), and new hydrogen atoms H(16C), H(16D), H(21C), and H(21D). The parameters of C(15b) and C(22b) could not be refined by least squares; their positions were taken from the difference maps, and their B's, as the average of those for C(15a) and C(22a). These last two atoms were refined with isotropic displacement parameters because refinement with anisotropic parameters was unsatisfactory. The parameters of the other atoms of the disorder were not refined.

Results and Discussion

Syntheses. There are several strategies for the synthesis of phi complexes that have been described, but in light of an increased interest for pharmacological applications, we sought improved methods of preparation.

Attempts to introduce the phi ligand by reaction of the chloro complexes $[Rh(N_4)Cl_2]^+$ with the phi precursor 9,10-diaminophenanthrene (DAP) followed by oxidation were not successful if N was an amino ligand ($N_4 = (NH_3)_4$, $(en)_2$, tren, [12]aneN$_4$), since the chloride ion is a particularly poor leaving group. Substitution of coordinated chloride may be accomplished by refluxing the chloro complexes $[Rh(en)_2Cl_2]Cl$, $[Rh(tren)Cl_2]Cl$, and $[Rh([12]aneN_4)Cl_2]Cl$ in aqueous NaOH for 30 min and, subsequently, adjusting the pH to 6.5 with perchloric acid to form the aquo complexes $[Rh(N_4)(H_2O)_2]^{3+}$. Without further isolation or purification, this solution is added to a dioxygen-free suspension of DAP in ethanol and the heterogenous reaction mixture is heated at reflux for 40 min to 5 h (eq 1). To avoid

$$[Rh(N_4)Cl_2]Cl \xrightarrow[3.\ DAP]{1.\ NaOH \quad 2.\ HClO_4 \quad 4.\ O_2} [Rh(N_4)phi]^{3+} \qquad (1)$$

N_4 = 2en, tren, [12]aneN$_4$

air-oxidation and subsequent decomposition, we excluded dioxygen rigorously during this reaction step. After cooling to room temperature, the reaction mixture is allowed to oxidize in air overnight. Precipitation by adding an aqueous solution of $NaClO_4$ or passing the crude reaction mixture through a Sephadex-SP cation-exchange column using dilute hydrochloric acid as eluent gives the complexes $[Rh(tren)phi](ClO_4)_3$, $[Rh(en)_2phi]Cl_3$, and $[Rh([12]aneN_4)phi]Cl_3$ in satisfactory to good yields (10–47%).

In addition to this two-step synthesis, most of the complexes are obtained in excellent yields in a one-pot synthesis starting from $RhCl_3$ by simply reversing the order of adding the ligands (eq 2). This new methodology offers the possibility of synthesizing

$$RhCl_3 \xrightarrow[3.\ O_2]{1.\ DAP \quad 2.\ N_4} [Rh(N_4)phi]^{3+} \qquad (2)$$

N_4 = 4NH$_3$, 2en, 2phen, 2bpy

$[Rh(N_4)phi]^{3+}$ complexes with a variety of different aliphatic or aromatic nitrogen coordinating ligands N in gram quantities. $[Rh(NH_3)_4phi]^{3+}$, for example, is better prepared using this single-step method than from *cis*-$[Rh(NH_3)_4Cl_2]^+$. Under rigorous exclusion of dioxygen, $RhCl_3$ hydrate is first reacted with 1 equiv of 9,10-diaminophenanthrene in water at 100 °C under argon with the resultant formation of a yellow precipitate. Dioxygen-free 30% NH_4OH is then added, and the reaction mixture is heated at reflux for 45 min. After air oxidation and Sephadex cation-exchange chromatography, $[Rh(NH_3)_4phi]Cl_3$ is obtained in high yield (59%).

Using the same synthetic strategy for the preparation of $[Rh(en)_2phi]^{3+}$ improved the yield substantially (55%). This reaction sequence is not limited to the more basic aliphatic ligands like ammonia and ethylenediamine. It is also very efficient for the synthesis of complexes $[RhAr_2phi]^{3+}$ or $[RhAr^1Ar^2phi]^{3+}$ with sterically more demanding and less basic aromatic ligands (Ar = 2,2′-bipyridine, 1,10-phenanthroline, and derivatives).[23] These ligands, however, require higher reaction temperatures and longer reaction times.

A modification in the two-step procedure was required in the case of $[Rh([12]aneS_4)phi]Cl_3$ (eq 3). Treatment of $[Rh([12]aneS_4)Cl_2]Cl$ with NaOH led to rapid decomposition. Interestingly, heating $[Rh([12]aneS_4)Cl_2]Cl$ and 1.1 equiv of DAP in ethanol/water 1:1 under exclusion of dioxygen for 25 min and subsequent air-oxidation gives the desired phi complex $[Rh([12]aneS_4)phi]Cl_3$ in excellent yield (71%).

$$[Rh([12]aneS_4)Cl_2]Cl \xrightarrow[2.\ O_2]{1.\ DAP} [Rh([12]aneS_4)phi]^{3+} \qquad (3)$$

Isomeric Purity. C_{18}-reversed-phase HPL-chromatography is a powerful tool to determine the chemical and isomeric purity of phi complexes of Rh(III). In the case of $[Rh([12]aneN_4)phi]^{3+}$, we obtained two baseline resolved peaks with capacity factors and relative peak areas at the detection wavelength of 254 nm of 5.4 (40%) for C_s-$[Rh([12]aneN_4)phi]^{3+}$ and 6.3 (60%) for C_{2v}-$[Rh([12]aneN_4)phi]^{3+}$ ($\alpha = 1.2$) (Figure S1). Collecting each isomer separately and lyophilizing and dissolving the yellow residue in water gave the same mixture of isomers due to rapid isomerization at high pH, indicative of a thermodynamic equilibrium. At higher pH, reprotonation may be sufficiently slow to permit conformational reorganization, leading to the equilibrium mixture. The difference in free energy between the all-exo conformation (A, Figure 2) and the exo, endo, exo, exo conformation of [12]aneN$_4$ (B, Figure 2) coordinated to Rh(III)

(23) Krotz, A. H. Unpublished results.

is 0.99 kJ/mol. However, the complexes were configurationally stable in the solution at low pH where deprotonation/reprotonation at the equatorial nitrogen is faster than inversion. No chromatographic evidence for the occurrence of any other isomer was obtained. In the case of the sulfur analogue $[Rh([12]aneS_4)phi]^{3+}$ we detected only one isomer displaying C_s-symmetry, indicating a large difference in free energy between this structure and the C_{2v}-symmetric structures A and C (Figure 2) (*vide infra*).

X-ray Crystallography of Phi Complexes of Rhodium(III). In our investigations of DNA recognition by metallointercalators a detailed knowledge of the geometry of the complexes is essential to understand the differences and similarities in the interactions ("recognition") with the base pairs in the major groove of double-stranded DNA. There are only two crystal structures of transition metal complexes with the 9,10-phenanthrenequinone diimine ligand described: $[Ru(bpy)_2phi](BF_4)_2 \cdot 0.19H_2O$[6] and *rac*-$[Rh(en)_2phi]Br_3 \cdot 3H_2O$.[24]

There has also been considerable interest in complexes of transition metals coordinated by macrocyclic polyamines and polythioethers. The thermodynamic and kinetic inertness together with the ability to stabilize unusual oxidation states [e.g. Rh(II)][25] has given rise to investigations of these complexes. It was of particular interest to us to compare and contrast how the small 12-membered cyclic tetraamine $[12]aneN_4$ and its sulfur analogue $[12]aneS_4$ would be coordinated in phi complexes of d^6 rhodium(III). The free ligands $[12]aneN_4$ and $[12]aneS_4$ have been characterized by X-ray crystal structure analyses.[26,27] A crystal structure of a rhodium(III) complex of $[12]aneS_4$, displaying coordination geometry B (Figure 2), has been reported,[32] but to our knowledge, no crystal structures of $[12]aneN_4$ coordinated to rhodium(III) have as yet been described. Due to the small ring size, macrocyclic ligands $[12]aneN_4$ and $[12]aneS_4$ coordinate to metals in a folded form at cis positions. From nine possible coordination geometries (due to two possible configurations of each of the coordinating atoms) six can be safely ruled out due to steric requirements. The remaining three isomers [(A) all-exo, (B) exo, endo, exo, exo, (C) exo, endo, exo, endo) are shown in Figure 2. Crystal structures of octahedral Co(III)[28] and Cr(III)[29] complexes coordinated by $[12]aneN_4$ showed only structure B. Interestingly, there are two crystal structures of $[12]aneN_4$ coordinated to Ni(II) in the literature; $[Ni([12]aneN_4)(H_2O)_2]_2(C_4O_4)(ClO_4)_2$ shows structure A,[30] and $[Ni([12]aneN_4)(H_2O)_2]_2(ClO_4)_2 \cdot H_2O$ shows structure B.[31]

Crystallographic studies of $[Rh(NH_3)_4phi]Cl_3$, $[Rh([12]aneN_4)phi](SCN)_3$, and $[Rh([12]aneS_4)phi]Br_3$ were undertaken, both to examine how the overall structure of the complexes is influenced by chelate ring puckering, relative configuration of coordinating atoms and the strain of coordinated macrocycles, and to provide structural data to evaluate the site-specific interactions of these complexes with duplex DNA. Suitable crystals for X-ray crystallography were obtained by slow evaporation of an aqueous solution of the chloride salt of the complex and an excess of the sodium or potassium salt of the corresponding counterion.

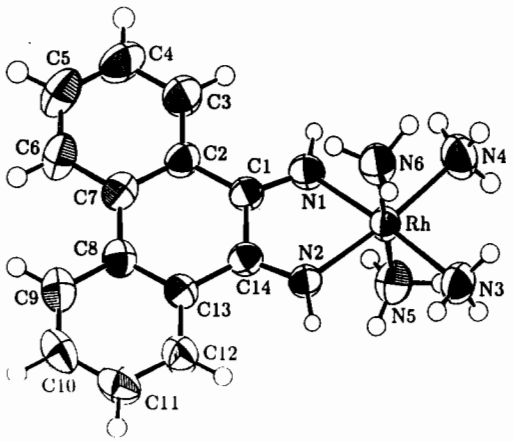

Figure 3. ORTEP drawing of the cation of $[Rh(NH_3)_4phi]Cl_3 \cdot H_2O$ with 75% probability ellipsoids showing the numbering system. Hydrogen atoms are shown as spheres with thermal parameters 20% those assigned.

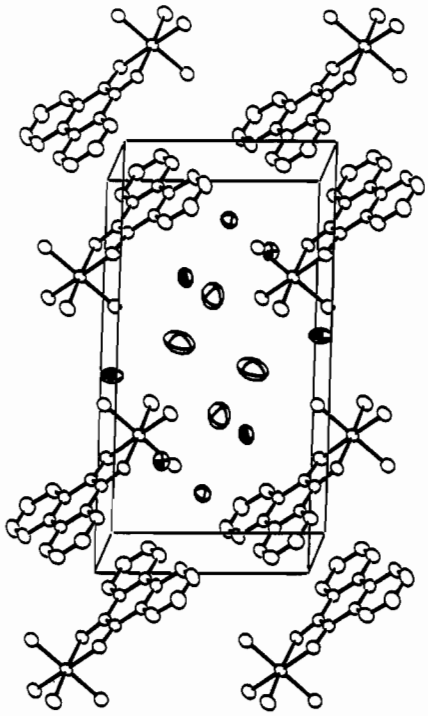

Figure 4. Contents of the unit cell of $[Rh(NH_3)_4phi]Cl_3 \cdot 3H_2O$ and some neighboring species. Atoms are shown as 50% probability ellipsoids; hydrogen atoms are omitted for clarity. Chloride ions have shaded octants, and water molecules have outlined octants. The view is perpendicular to the *bc* plane.

Crystal Structure of $[Rh(NH_3)_4phi]Cl_3 \cdot 3H_2O$. An ORTEP[33] diagram of the structure of the cation $[Rh(NH_3)_4phi]^{3+}$ with the atomic numbering scheme is displayed in Figure 3; the contents of the unit cell and some neighboring species are shown in Figure 4. Table II contains selected bond distances and angles. Table III shows selected interionic and intermolecular distances less than 3.5 Å indicating possible hydrogen bonds. The atom positional and thermal parameters arising from the structure determination and complete tables of bond distances and angles and distances less than 3.5 Å are provided as supplementary material.

The rhodium(III) ion is in an octahedral environment, coordinated by four NH_3 molecules and two imine nitrogens of the chelating phi ligand. The NH_3 groups occupy ideal octahedral positions with N–Rh–N angles between 88.9(1) and 91.6(1)° between cis-coordinated groups and 179.3(1)° between the axial

(24) Schaefer, W. P.; Krotz, A. H.; Kuo, L. Y.; Shields, T. P.; Barton, J. K. *Acta Crystallogr.* **1992**, *48*, 2071.
(25) Cooper, S. R.; Rawle, S. C.; Yagbasan, R.; Watkin, D. J. *J. Am. Chem. Soc.* **1991**, *113*, 1600.
(26) Reibenspies, J. H.; Anderson, O. P. *Acta Crystallogr.* **1990**, *C46*, 163.
(27) Wolf, R. E., Jr.; Hartman, J. R.; Storey, J. M. E.; Foxman, B. M.; Cooper, S. R. *J. Am. Chem. Soc.* **1987**, *109*, 4328.
(28) Kojima, M.; Nakabayashi, K.; Ohba, S.; Okumoto, S.; Saito, Y.; Fujita, J. *Bull. Chem. Soc. Jpn.* **1986**, *59*, 277 and references cited therein.
(29) Hodgson, D. J.; Pedersen, E.; Toftlund, H.; Weiss, C. *Inorg. Chim. Acta* **1986**, *120*, 177.
(30) Bencini, A.; Bianchi, A.; Garcia-España, E.; Jeannin, Y.; Julve, M.; Marcelino, V.; Philoche-Levisalles, M. *Inorg. Chem.* **1990**, *29*, 963.
(31) Scott, B.; Brewer, K. J.; Spreer, L. O.; Craig, C. A.; Otvos, J. W.; Calvin, M.; Tayler, S. *J. Coord. Chem.* **1990**, *21*, 307.
(32) Blake, A. J.; Schröder, M. *Adv. Inorg. Chem.* **1990**, *35*.
(33) Johnson, C. K. ORTEPII. Report ORNL-3794, 3rd revision, Oak Ridge National Laboratory, Oak Ridge, TN, 1976.

Table II. Selected Distances (Å) and Angles (deg) in $[Rh(NH_3)_4phi]^{3+}$, C_s-and C_{2v}-$[Rh([12]aneN_4)phi]^{3+}$, and $[Rh([12]aneS_4)phi]^{3+}$

		$[Rh(NH_3)_4phi]^{3+}$	
		Distances	
Rh–N(1)	2.002(2)	Rh–N(4)	2.075(3)
Rh–N(2)	2.010(2)	Rh–N(5)	2.073(3)
Rh–N(3)	2.082(3)	Rh–N(6)	2.061(2)
		Angles	
N(1)–Rh–N(2)	77.6(1)	N(2)–Rh–N(6)	89.1(1)
N(1)–Rh–N(3)	173.7(1)	N(3)–Rh–N(4)	89.5(1)
N(1)–Rh–N(4)	96.6(1)	N(3)–Rh–N(5)	90.3(1)
N(1)–Rh–N(5)	91.2(1)	N(3)–Rh–N(6)	89.5(1)
N(1)–Rh–N(6)	89.0(1)	N(4)–Rh–N(5)	88.9(1)
N(2)–Rh–N(3)	96.2(1)	N(4)–Rh–N(6)	90.4(1)
N(2)–Rh–N(4)	174.2(1)	N(5)–Rh–N(6)	179.3(1)
N(2)–Rh–N(5)	91.6(1)		
		$[Rh([12]aneN_4)phi]^{3+}$	
		Distances	
Rh–N(1)	2.007(6)	Rh–N(4)	2.068(6)
Rh–N(2)	2.026(6)	Rh–N(5)	2.021(6)
Rh–N(3)	2.026(7)	Rh–N(6)	2.067(7)
		Angles	
N(1)–Rh–N(2)	76.8(3)	Rh–N(3)–C(15A)	107.4(6)
N(1)–Rh–N(3)	171.8(3)	Rh–N(3)–C(22A)	108.1(6)
N(1)–Rh–N(4)	99.1(3)	Rh–N(3)–C(15B)	116.2
N(1)–Rh–N(5)	91.6(3)	Rh–N(3)–C(22B)	115.3
N(2)–Rh–N(3)	95.2(3)	Rh–N(4)–C(16)	108.5(5)
N(2)–Rh–N(4)	95.0(2)	Rh–N(4)–C(17)	106.2(5)
N(2)–Rh–N(5)	168.1(2)	Rh–N(5)–C(18)	109.9(5)
N(2)–Rh–N(6)	100.2(3)	Rh–N(5)–C(19)	111.1(5)
N(3)–Rh–N(4)	82.9(3)	Rh–N(6)–C(20)	107.5(5)
N(3)–Rh–N(5)	96.5(3)	Rh–N(6)–C(21)	108.8(5)
N(3)–Rh–N(6)	82.5(3)	C(22A)–N(3)–C(15A)	120.5(8)
N(1)–Rh–N(6)	97.3(3)	C(22B)–N(3)–C(15B)	113.6(14)
N(4)–Rh–N(5)	84.5(3)	C(17)–N(4)–C(16)	111.7(6)
N(4)–Rh–N(6)	159.8(3)	C(19)–N(5)–C(18)	119.5(6)
N(5)–Rh–N(6)	83.4(3)	C(21)–N(6)–C(20)	112.4(7)
		$[Rh([12]aneS_4)phi]^{3+}$	
		Distances	
Rh–N(1)	2.029(7)	Rh–S(2)	2.292(3)
Rh–N(2)	2.065(7)	Rh–S(3)	2.355(3)
Rh–S(1)	2.373(3)	Rh–S(4)	2.302(3)
		Angles	
N(1)–Rh–N(2)	77.2(3)	N(2)–Rh–S(4)	97.3(2)
N(1)–Rh–S(1)	96.5(2)	Rh–S(1)–C(15)	100.5(3)
N(1)–Rh–S(2)	91.8(2)	Rh–S(1)–C(22)	102.2(3)
N(1)–Rh–S(3)	93.6(2)	Rh–S(2)–C(16)	101.6(3)
N(1)–Rh–S(4)	174.1(2)	Rh–S(2)–C(17)	102.1(3)
N(2)–Rh–S(1)	93.1(2)	Rh–S(3)–C(18)	101.8(3)
N(2)–Rh–S(2)	168.9(2)	Rh–S(3)–C(19)	103.1(3)
N(2)–Rh–S(3)	94.4(2)	Rh–S(4)–C(20)	99.0(3)
S(1)–Rh–S(2)	87.3(1)	Rh–S(4)–C(21)	99.0(3)
S(1)–Rh–S(3)	168.5(1)	C(15)–S(1)–C(22)	100.4
S(1)–Rh–S(4)	85.6(1)	C(16)–S(2)–C(17)	107.0
S(2)–Rh–S(3)	87.1(1)	C(18)–S(3)–C(19)	100.3
S(2)–Rh–S(4)	93.8(1)	C(20)–S(4)–C(21)	108.3
S(3)–Rh–S(4)	84.8(1)		

ammine nitrogen atoms. Angles in the equatorial plane involving the imine nitrogens differ from the ideal octahedral values due to the intrinsically small bite-angle of the bis(imine) ligand [77.6(1)°]. $Rh–N_{NH_3}$ distances (2.061(2)–2.082(3) Å) are identical to those reported for $[Rh(NH_3)_6]^{3+}$ (2.069 Å) and are slightly longer than $Rh–N_{imine}$–bond distances (2.002(2), 2.010(2) Å) most likely due to the different hybridizations of the nitrogen donors (e.g. the Rh–N distance in $[Rh(bpy)_3](PF_6)_3$ is 2.015 Å).[34] C–N and C–C bond distances in the phi ligand are as expected with C=N distances of 1.282 and 1.283 Å. Intermolecular hydrogen-bond contacts occur among the NH_3 and NH groups, the water molecules, and the chloride ions.

(34) Hauser, A.; Mäder, M.; Robinson, W. T.; Murugesan, R.; Ferguson, J. *Inorg. Chem.* **1987**, *26*, 1331.

Table III. Intermolecular and Interionic Distances Less Than 3.5 Å Indicating Hydrogen Bonding

		$[Rh(NH_3)_4phi]Cl_3·3H_2O$	
N(1)–Cl(1)	3.309(2)	N(5)–W(2)	3.117(5)
N(1)–Cl(2)	3.204(2)	N(6)–Cl(2)	3.278(3)
N(3)–Cl(1)	3.397(3)	N(6)–Cl(2)	3.286(3)
N(3)–W(3)	3.179(6)	N(6)–Cl(3)	3.272(3)
N(3)–Cl(3)	3.374(3)	Cl(1)–W(1)	3.151(3)
N(4)–W(3)	3.389(6)	Cl(2)–W(3)	3.312(5)
N(4)–Cl(2)	3.327(3)	Cl(3)–W(2)	3.220(4)
N(4)–Cl(2)	3.478(3)	Cl(3)–W(3)	3.192(5)
N(4)–W(2)	2.984(5)	Cl(3)–W(1)	3.259(3)
N(5)–W(1)	3.004(3)	W(2)–W(3)	2.974(6)
N(5)–Cl(1)	3.326(3)		
		$[Rh([12]aneN_4](SCN)_3·2H_2O$	
N(2)–N(7)	2.927(13)	O(1)–O(2)	2.70(2)
N(3)–O(1)	2.893(14)	O(1)–N(10A)	2.954
N(4)–S(1)	3.261(7)	O(1)–S(4B)	2.954
N(5)–N(8)	2.984(10)	O(1)–O(1)	2.738(17)
N(6)–S(2)	3.276(7)	O(1)–O(2)	3.42(2)
S(2)–O(2)	3.399(17)	O(2)–N(10A)	2.940
N(9)–O(2)	2.97(2)	O(2)–S(4B)	2.940
N(9)–O(1)	2.72(2)		
		$[Rh([12]aneS_4)phi]Br_3·3H_2O$	
N(1)–Br(3)	3.308(7)	Br(2)–W(1)	3.344(7)
N(2)–W(1)	3.125(10)	W(1)–W(3)	2.837(11)
S(3)–W(1)	3.309(8)	Br(2)–HN(1)	2.815
Br(1)–W(2)	3.389(8)	Br(3)–HN(2)	2.977
Br(1)–W(3)	3.301(8)	Br(3)–HN(1)	2.748
Br(1)–W(2)	3.319(8)	W(1)–HN(2)	3.035
Br(2)–W(3)	3.348(8)		

Crystal Structure of $[Rh([12]aneN_4)phi](SCN)_3·2H_2O$. From an aqueous solution of a mixture of isomers C_{2v}-$[Rh([12]aneN_4)phi]Cl_3$ and C_s-$[Rh([12]aneN_4)phi]Cl_3$ (ratio 60:40) and potassium thiocyanate, red crystals were obtained by slow evaporation at room temperature. ORTEP[33] diagrams of the structures of the two different cations $[Rh([12]aneN_4)phi]^{3+}$ with the atom-numbering scheme are displayed in Figure 5A,B. Tables II–IV contain selected bond distances and bond angles, hydrogen-bonding distances, and torsion angles, respectively. The atom positional and thermal parameters arising from the structure determination and complete tables of bond distances and angles and distances less than 3.5 Å are provided as supplementary material.

The crystal used for the X-ray diffraction studies consisted of two distinguishable monomeric cations $[Rh([12]aneN_4)phi]^{3+}$, noncoordinated thiocyanate ions, and lattice water molecules. The two isomers differ due to an inverse configuration at the equatorial nitrogen N(3). The isomer, given in Figure 5A, which data refinement indicates to be in the crystal in a population of 84%, has approximate C_s symmetry with the plane of symmetry passing through the metal center and the imine nitrogens. Due to the small size, the macrocycle is coordinated around the metal center in a folded manner showing an exo–endo–exo–exo arrangement (B, Figure 2). The chiral conformations of the four five-membered rings N–C–C–N–Rh (I–IV) are δ, λ, λ, δ, respectively. The minor isomer (Figure 5B), as refined in the crystal structure in a population of 16%, has an approximate C_{2v} symmetry with one plane of symmetry passing through the metal center and the imine nitrogens and one plane passing through the Rh center and the two axial amine nitrogens. The macrocycle is folded around the metal center in an all-exo arrangement (A, Figure 2) with all hydrogens attached to a nitrogen on the same side of an idealized plane through nitrogen atoms of the macrocycle. The chiral conformations of the four five-membered chelate rings N–C–C–N–Rh (I–IV) are λ, δ, λ, δ. Differences in bond angles or bond lengths between the two isomers are only seen at atoms near N(3) [C(15a) and C(22a) versus C(15b) and C(22b)].

The coordination geometry around the rhodium in both isomers is a distorted octahedron with four coordination sites occupied

Table IV. Torsion Angles (deg) of the Aliphatic Ligands in Λ-[Rh(en)$_2$phi]Br$_3$·3H$_2$O, C_s- and C_{2v}-[Rh([12]aneN$_4$)phi]SCN)$_3$·2H$_2$O, and [Rh([12]aneS$_4$)phi]Br$_3$·3H$_2$O

	Λ-[Rh(en)$_2$phi]$^{3+}$		
N(6)–C(18)–C(17)–N(5)[a]	50.7	N(4)–C(16)–C(15)–N(3)[b]	–49.2
	C_s-[Rh([12]aneN$_4$)phi]$^{3+}$		
N(6)–C(20)–C(19)–N(5)[a]	–52.2	N(4)–C(16)–C(15A)–N(3)[b]	38.3
C(20)–C(19)–N(5)–C(18)	170.6	C(16)–C(15A)–N(3)–C(22A)	–169.2
C(19)–N(5)–C(18)–C(17)	–168.3	C(15A)–N(3)–C(22A)–C(21)	172.4
N(5)–C(18)–C(17)–N(4)[b]	52.0	N(3)–C(22A)–C(21)–N(6)[a]	–39.8
C(18)–C(17)–N(4)–C(16)	79.2	C(22A)–C(21)–N(6)–C(20)	128.6
C(17)–N(4)–C(16)–C(15A)	–131.4	C(21)–N(6)–C(20)–C(19)	–80.6
	C_{2v}-[Rh([12]aneN$_4$)phi]$^{3+}$		
N(6)–C(20)–C(19)–N(5)[a]	–52.2	N(4)–C(16)–C(15B)–N(3)[a]	–43.6
C(20)–C(19)–N(5)–C(18)	170.6	C(16)–C(15B)–N(3)–C(22B)	172.5
C(19)–N(5)–C(18)–C(17)	–168.3	C(15B)–N(3)–C(22B)–C(21)	–171.3
N(5)–C(18)–C(17)–N(4)[b]	52.0	N(3)–C(22B)–C(21)–N(6)[b]	44.0
C(18)–C(17)–N(4)–C(16)	79.2	C(22B)–C(21)–N(6)–C(20)	81.2
C(17)–N(4)–C(16)–C(15B)	–88.5	C(21)–N(6)–C(20)–C(19)	–80.6
	[Rh([12]aneS$_4$)phi]$^{3+}$		
S(1)–C(15)–C(16)–S(2)[b]	–58.1	S(3)–C(19)–C(20)–S(4)[a]	54.5
C(15)–C(16)–S(2)–C(17)	161.7	C(19)–C(20)–S(4)–C(21)	–164.8
C(16)–S(2)–C(17)–C(18)	–159.8	C(20)–S(4)–C(21)–C(22)	163.4
S(2)–C(17)–C(18)–S(3)[a]	55.3	S(4)–C(21)–C(22)–S(1)[b]	–54.3
C(17)–C(18)–S(3)–C(19)	78.0	C(21)–C(22)–S(1)–C(15)	123.4
C(18)–S(3)–C(19)–C(20)	–124.5	C(22)–S(1)–C(15)–C(16)	–74.1

[a] Chelate ring is puckered in δ-conformation. [b] Chelate ring is puckered in λ-conformation.

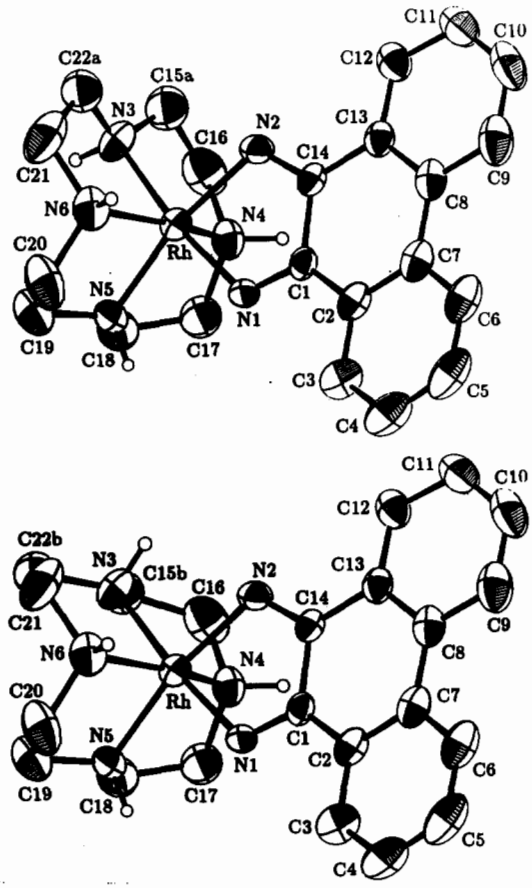

Figure 5. ORTEP drawing of the C_s-symmetric cation (A, top) and the C_{2v}-symmetric cation (B, bottom) of [Rh([12]aneN$_4$)phi](SCN)$_3$·2H$_2$O with 50% probability ellipsoids showing the numbering system. Hydrogen atoms on N(3), N(4), N(5), and N(6) are shown as spheres with thermal parameters 10% those assigned; other hydrogen atoms are omitted for clarity.

in a cis-arrangement by the four nitrogens of the folded tetraazamacrocycle and two sites coordinated by two imine nitrogens of the phi ligand. The N(1)–Rh–N(2) angle of 76.8(3)° is due to the small bite of the phi ligand. The bite angles N–Rh–N of the tetraazamacrocycle average 83.8° with actual values between 82.5 and 84.5°. They are only slightly larger

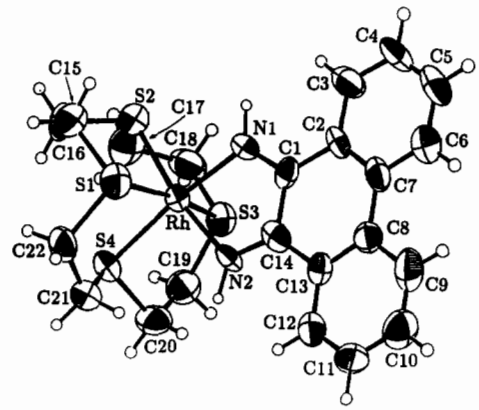

Figure 6. ORTEP drawing of the cation of [Rh([12]aneS$_4$)phi]Br$_3$·3H$_2$O with 80% probability ellipsoids showing the numbering system. Hydrogen atoms are shown as spheres with thermal parameters 10% those assigned.

than those observed in the less strained ethylenediamine complex (82.9, 83.3°).[24] The considerable distortion is best seen in the N(4)–Rh–N(6) angle of 159.8(3)° and the N(3)–Rh–N(5) angle of 96.5(3)°. Most of the Rh–N–C angles of the macrocycle range from 106.2(5) to 111.1(5)°. Exceptions are the Rh–N(3)–C(15B) and Rh–N(3)–C(22B) angles in the C_{2v}-symmetric isomer with angles of 116.2 and 115.3°, respectively. C–N$_{ax}$–C angles are 111.7(6) and 112.4(7)°, respectively, but angles C–N$_{eq}$–C show a significant distortion and are as large as 119.5(6)° for C(19)–N(5)–C(18) and 120.5(8)° for C(22A)–N(3)–C(15A) in isomer A. This observation has been made in other crystal structures of [12]aneN$_4$ coordinated to metal ions.[28,29]

Rh–N$_{imine}$-bond lengths are in the same range as reported for other phi complexes of rhodium. Rh–N$_{ax}$ bond lengths (2.067(7), 2.068(6) Å) are slightly longer than Rh–N$_{eq}$ bond lengths (2.021(6), 2.026(6) Å). This is also apparent in the crystal structure of [Rh([12]aneS$_4$)phi]$^{3+}$ (*vide infra*). Bond lengths within the phi ligand are as expected.

Crystal Structure of [Rh([12]aneS$_4$)phi]Br$_3$·3H$_2$O. An ORTEP[33] diagram of the structure of the cation of [Rh([12]aneS$_4$)phi]Br$_3$·3H$_2$O with the atomic numbering scheme is displayed in Figure 6. Tables II–IV contain selected bond distances and angles, hydrogen-bonding distances, and torsion angles, respectively. The atom positional and thermal parameters arising from the structure

determination and complete tables of bond distances and angles and distances less than 3.5 Å are provided as supplementary material.

The crystal consists of one monomeric $[Rh([12]aneS_4)phi]^{3+}$ species, bromide ions, and lattice water molecules. The coordination geometry around the rhodium(III) cation is a slightly distorted octahedron. The cation possesses an approximate C_s symmetry with the mirror plane passing through the metal center and the imine nitrogens. The rhodium(III) is coordinated to the folded tetrathia macrocycle via the four sulfur atoms and to the bidentate aromatic phi ligand via the two imine nitrogens. The macrocyclic thioether adopts an exo, endo, exo, exo conformation as seen[32] in *cis*-$[RhCl(PEt_2Ph)([12]aneS_4)]^{2+}$ but in contrast to its all-exo conformation in the noncoordinated state. The chiral conformations of the puckered five-membered rings S-C-C-S-Rh (I–IV) are δ, λ, λ, and δ, respectively.

Analysis of the torsion angles (Table IV) showed gauche conformations for all four S–C–C–S torsional angles with angles between 54.3 and 58.1°. This is in contrast to the noncoordinated form of $[12]aneS_4$, where anti conformations of S–C–C–S units with torsion angles of 173° are preferred to avoid unfavorable repulsive gauche interactions. Four of eight C–S–C–C torsional angles show an anti conformation (angles between 159.8 and 164.8°). Angles around the metal center range from 77.2(3)° for the bite angle [N(1)–Rh–N(2)] of phi to 97.3(2)° for the angle N(2)–Rh–S(4). The bite angles of the tetradentate thiamacrocycle average 86.2° with actual values between 84.8(1) and 87.3(1)° compared to 83.8° in the nitrogen analogue. Deviations from ideal octahedral geometry are also seen in the S(2)–Rh–S(4) and S(1)–Rh–S(3) angles (93.8(1), 168.5(1)°). $C–S_{eq}–C$ angles (107.0, 108.3°) are close to the tetrahedral value; however, $C–S_{ax}–C$ angles are as small as 100.4°. $Rh–S_{ax}$ bond distances [2.373(3), 2.355(3) Å] are significantly longer than $Rh–S_{eq}$ bond distances (2.292(3), 2.302(3) Å). C–S bond lengths range from 1.795(10) Å for S(2)–C(17) to 1.856(10) Å for S(1)–C(22). Bond lengths within the phi ligand are as expected.

Crystal Packing. The tendency of aromatic heterocyclic systems to form aggregates via π-stacking is probably best illustrated in the double-helical structure of DNA. The crystal packing of $[Rh(NH_3)_4phi]^{3+}$, shown in Figure 4, shows partial overlap of the phi ligands in dimer pairs at a distance of 3.4 Å. An extended stack of phi ligands is not evident in the crystal, however, likely owing to the bulk of the octahedral geometry. $[Rh([12]aneN_4)phi]^{3+}$ and $[Rh([12]aneS_4)phi]^{3+}$ also show partial overlap of the π-systems (see supplementary material) but, consistent with the presence of more bulky ancillary ligands, to a lesser extent. The crystal packing represents the balance between the propensity of the aromatic ligands for π-stacking and crystal packing forces.

Topological Comparisons among the Coordination Complexes. In order to explore the differences in the DNA recognition characteristics of the phi complexes, we analyzed the spatial positions of the atoms of the ancillary ligands. The differences in structure and shape of the complexes are caused by several factors: the chirality of the complex (Δ, Λ), the chiral conformation of the chelate rings XCCXRh (δ, λ), the configuration of the equatorial coordinating atoms (syn, anti), the strain of the ligands, and the bond lengths (S–Rh, –C versus N–Rh, –C).

In order to compare the topology of the complexes, we transformed the coordinates into a system that has its origin in the rhodium center. The distances of the ancillary ligand atoms of the complexes $[Rh(NH_3)_4phi]^{3+}$, Λ- and Δ-$[Rh(en)_2phi]^{3+}$, C_s- and C_{2v}-$[Rh([12]aneN_4)phi]^{3+}$, and $[Rh([12]aneS_4)phi]^{3+}$ to three planes A, B, and C are compared (Table S16). For each complex, plane A is defined by Rh, $N1_{imine}$, and $N2_{imine}$. Plane B is perpendicular to plane A passing through Rh and the middle of the connection of $N1_{imine}$ and $N2_{imine}$. Plane C is perpendicular to planes A and B and passes through the rhodium center. The numbering system and the planes A–C are schematically shown in Figure 2.

Comparisons may be made among these crystal structures more easily using this metal-centered coordinate system. For example, to avoid energetically unfavored eclipsed conformations, the five-membered chelate rings N-C-C-N-Rh in $[Rh(en)_2phi]^{3+}$ pucker in two chiral conformations. In the solid state, one chelate ring adopts the λ-conformation and the other adopts the δ-conformation. Both rings are independent from each other, and the energy barrier between the two conformations is low enough so that in solution a change from the δ- to λ-conformations can easily be accomplished. In the Λ-enantiomer this conformational change (δ to λ) shifts C(2) about 0.5 Å away from plane B and 0.6 Å closer to plane C. The separation is 0.78 Å. C(3) is shifted 0.4 Å toward plane B and 0.3 Å away from plane C. The separation is 0.52 Å.

The tetradentate macrocyclic ligands $[12]aneN_4$ and $[12]aneS_4$ are coordinated in a folded manner around the rhodium. There is little conformational freedom in the four fused five-membered chelate rings. The chiral conformation of each chelate ring is determined by the relative configuration of the coordinating atoms in the equatorial plane. As a consequence, chelate rings at pro-*S* positions (e.g. C(3), C(2), X(1) and C(9), C(8), X(7) in C_{2v}-$[Rh([12]aneN_4)phi]^{3+}$ and C(5), C(6), X(7) in C_s-$[Rh([12]aneN_4)phi]^{3+}$ and $[Rh([12]aneS_4)phi]^{3+}$) of the prochiral atoms X(4) and X(10) are always puckered in a λ-conformation and chelate rings at pro-*R* positions (e.g. C(5), C(6), X(7) and C(11), C(12), X(1) in C_{2v}-$[Rh([12]aneN_4)phi]^{3+}$ and C(3), C(2), X(1) in *C s*-$[Rh([12]aneN_4)phi]^{3+}$ and $[Rh([12]aneS_4)phi]^{3+}$) are always puckered in δ-conformations.

The strain in complexes with folded macrocycles is best seen in angles X(1)–Rh–X(7) between axial coordinating atoms (159.8° in $[Rh([12]aneN_4)phi]^{3+}$, 168.5° in $[Rh([12]aneS_4)phi]^{3+}$) and angles X(4)–Rh–X(10) between equatorial coordinating atoms (96.5° in $[Rh([12]aneN_4)phi]^{3+}$, 97.3° in $[Rh([12]aneS_4)phi]^{3+}$), which differ substantially from ideal octahedral angles. As a consequence, carbon atoms in $[Rh([12]aneN_4)phi]^{3+}$ are about 0.1–0.2 Å closer to plane A than in $[Rh(en)_2phi]^{3+}$.

Differences between C_s-$[Rh([12]aneS_4)phi]^{3+}$ and C_s-$[Rh([12]aneN_4)phi]^{3+}$ are mainly consequences of the increased bond lengths to S compared to N. Rhodium–sulfur bond lengths average 2.33 Å (Rh–N = 2.05 Å), and carbon–sulfur bond lengths average 1.82 Å (N–C = 1.48 Å). Bond angles within the sulfur and the nitrogen macrocycle are also substantially different. $C–S_{ax}–C$ angles (100.4°) are much smaller than $C–N_{ax}–C$ angles of 112°. $C–S_{eq}–C$ angles are 107.6° compared to $C–N_{eq}–C$ of 120°. As a consequence, most atoms in $[Rh([12]aneS_4)phi]^{3+}$ are about 0.2–0.3 Å further away from plane A than corresponding atoms in $[Rh([12]aneN_4)phi]^{3+}$, except C(3), X(4), and X(10). Carbon atoms C(2), C(3), C(5), and C(6) at the S_{anti}-side are 0.15–0.6 Å further away from plane B than in the N-analogue, but on the S_{syn}-side C(9), C(11), and C(12) are 0.1–0.4 Å closer to plane B than in the N-analogue. Carbon atoms C(2), C(3), C(5), and C(6) at the S_{anti}-side are up to 0.2 Å closer to plane C than in the N-analogue, but on the S_{syn}-side C(9), C(11), and C(12) are about 0.5 Å further away from plane C than in the N-analogue.

The coordination geometry of the tetradentate 12-membered macrocycles around a metal ion is of particular interest, since three conformations shown in Figure 2 seem to be equally likely. The C_s- and C_{2v}-symmetric isomers of $[Rh([12]aneN_4)phi]^{3+}$ differ only slightly in energy (0.99 kJ/mol), but we did not detect an isomer of structure C (Figure 2) most likely due to two close hydrogen contacts C(2)-H···H-C(12) and C(6)-H···H-C(8). In the crystal structures the angle $C–N_{ax}–C$ is about 111–112°; however, the equatorial $C–N_{eq}–C$ angles are about 120° in order to avoid close hydrogen contacts between methylene groups

Table V. Chemical Shifts of Aromatic Protons of Phi Complexes of Rhodium(III)[a]

complex	chem shifts, ppm (multiplicity, no. of hydrogens)			
$[Rh(NH_3)_4phi]^{3+}$		8.22 (d, 2H), 8.14 (d, 2H)	7.66 (dd, 2H)	7.48 (dd, 2H)
$[Rh(en)_2phi]^{3+}$		8.17 (d, 2H), 8.15 (d, 2H)	7.69 (dd, 2H)	7.49 (dd, 2H)
$[Rh(tren)phi]^{3+}$	8.50 (d, 1H)	8.15 (m, 3H)	7.70 (m, 2H)	7.50 (m, 2H)
$[Rh([12]aneN_4)phi]^{3+}$ [b]	8.50 (d, <1H)	8.2 (m, >7H)	7.67 (m, 4H)	7.50 (m, 4H)
$[Rh([12]aneS_4)phi]^{3+}$	8.54 (d, 1H)	8.21 (d, 1H), 8.12 (2d, 2H)	7.65 (2dd, 2H)	7.49 (2dd, 2H)

[a] The spectra were recorded at 300 MHz in D_2O. [b] A mixture of isomers (40:60, according to HPLC); the integration at 8.50 and 8.2 suggests that the minor isomer has C_s symmetry.

connected to the N_{eq}. The necessary changes in bond angles in order to avoid close transannular contacts would obviously raise the energy of an exo, endo, exo, endo isomer to such an extent, compared to the two isolated isomers, that no detectable amounts of this isomer are formed.

Only one isomer of $[Rh([12]aneS_4)phi]^{3+}$ with C_s symmetry (B, Figure 2) is observed. Molecular modeling using the data from the crystal structure analysis shows close transannular hydrogen contacts between C(3)-H···H-C(11) and C(5)-H···H-C(9) in a complex with structure A. Due to the increased bond lengths the calculated distances between the two hydrogens would be only about 1.2 Å, compared to 2.0 Å for isolated C_{2v}-$[Rh([12]aneN_4)phi]^{3+}$, and would result in transannular repulsion. However, modeling of a theoretical complex $[Rh([12]aneS_4)phi]^{3+}$ with structure C does not show close hydrogen–hydrogen contacts. Investigation of interactions between heteroatoms,[35] e.g. conformational analysis of compounds with X–C–C–X structural elements (X = N, O, F or S, Cl) showed that if X is a first-row element, gauche conformations are preferred due to 1,4-interactions, which are stabilized by dispersion forces ("attractive gauche effect"). In contrast, it was found, that second-row elements prefer anti conformations due to electron–electron repulsion, which destabilizes gauche conformations ("repulsive gauche effect"). In $[Rh([12]aneS_4)phi]^{3+}$ with structure C, the distance between the two sulfur atoms in the equatorial plane is about 3.4 Å. The fact that we could not detect this isomer is, therefore, most likely due to electron–electron repulsion destabilizing this isomer.

NMR Spectroscopy. ^1H- and ^{13}C-NMR spectroscopy confirmed that the structures of the complex cations seen in the solid state are retained in solution with respect to constitution and symmetry. In complexes containing en, tren, $[12]aneN_4$, or $[12]aneS_4$ the resonances of the ancillary ligands (3–4 ppm) are well separated from the resonances of the phi ligand (7.5–8.5 ppm, Table V). Hydrogen resonances at C(2), C(3), C(6), and C(7) are found at 7.5 and 7.7 ppm and at C(1), C(4), C(5), and C(8) are found at 8.2 ppm in symmetric complexes $[Rh(NH_3)_4phi]^{3+}$ and $[Rh(en)_2phi]^{3+}$. However, in complexes $[Rh(tren)phi]^{3+}$, C_s-$[Rh([12]aneN_4)phi]^{3+}$, and $[Rh([12]aneS_4)phi]^{3+}$ (C_s symmetry) with an anti-configuration at one equatorial coordinated atom, one aromatic proton (at C(1) or C(8)) is shifted downfield to 8.5 ppm. This characteristic shift can be used to distinguish between syn and anti configurations at the equatorial positions to determine the conformation of coordinated macrocycles in solution or the configuration of secondary amines.[11] The ^1H-NMR spectrum of $[Rh([12]aneN_4)phi]^{3+}$ clearly shows a mixture of two isomers, with one doublet, integrating for less than one proton, shifted to 8.5 ppm. In the proton-decoupled ^{13}C-NMR spectrum (Figure S1) two sets of resonances can be distinguished due to the different height of the signals. One set shows the expected pattern of a $[12]aneN_4$ complex of lower symmetry C_s (B, Figure 2) with four aliphatic, twelve aromatic (some signals are overlapping with the other set of signals), and two imino-carbonyl resonances. The second set of resonances showed the expected pattern for a phi complex with higher symmetry C_{2v} with two aliphatic, six aromatic, and one imino-carbonyl resonances. The ^{13}C-NMR data do not allow one to distinguish between structures A and C (Figure 2); however, the chemical shifts of the phi protons (at C(1) and C(8)) in the ^1H-NMR spectrum suggest structure A for the C_{2v}-symmetric isomer. Further evidence for this assignment is obtained from the X-ray crystallographic studies and our modeling studies.

^1H- and ^{13}C-NMR analyses of $[Rh([12]aneS_4)phi]^{3+}$ were indicative of structure B (Figure 2) in solution, which is also seen in the solid state. The proton spectrum shows a nonsymmetric phi pattern in the aromatic region with one doublet, integrating for one proton shifted to 8.5 ppm. The proton-decoupled ^{13}C-NMR spectrum shows the expected pattern for a complex with a plane of symmetry passing through the rhodium and the imine nitrogens. In contrast to the nitrogen analogue, spectroscopy and HPLC did not give any evidence for the occurrence of more than one isomer.

The ^1H-NMR spectrum of $[Rh(NH_3)_4phi]^{3+}$ (point group C_{2v}) recorded in DMSO-d_6 shows in addition to the aromatic protons a broad signal for the imine protons at 14.2 ppm and two signals at 4.6 and 3.75 ppm (6H each) of the axial and equatorial ammine groups.

Electronic Absorption Spectroscopy. The electronic absorption spectra of the polyamine complexes $[Rh(NH_3)_4phi]^{3+}$, $[Rh(en)_2phi]^{3+}$, $[Rh(tren)phi]^{3+}$, and $[Rh([12]aneN_4)phi]^{3+}$ (two isomers) display a characteristic shape in the wavelength range between 250 and 500 nm. They are characterized by a broad absorption band with a maximum and shoulders between 360 and 420 nm ($\epsilon = (1–1.5) \times 10^4\ M^{-1}\ cm^{-1}$), a shoulder near 290 nm, and three absorption maxima between 250 and 280 nm ($\epsilon \sim 2.5 \times 10^4\ M^{-1}\ cm^{-1}$) at pH 7. The electronic absorption spectra of $[Rh(en)_2phi]^{3+}$ and $[Rh([12]aneS_4)phi]^{3+}$ as a function of pH are shown in Figure 7, and the spectrum of $[Rh([12]aneN_4)phi]^{3+}$ is shown in Figure 8. In the spectrum of $[Rh([12]aneS_4)phi]^{3+}$ there is, in addition to the low-energy maximum at 359 nm, a well-pronounced shoulder at 331 nm.

There is a clear change in spectra of the phi coordination complexes as a function of protonation state of the coordinated phi ligand. Similar observations have been reported for aromatic analogues $[Rh(phen)_2phi]^{3+}$ and $[Rh(phi)_2bpy]^{3+}$.[6] In addition to a blue shift of maxima and shoulders, there is a substantial drop in intensity (10–30%) over the pH range pH 2–11 (Figure 7). Isosbestic points are observed at 268 and 333 nm for $[Rh(NH_3)_4phi]^{3+}$, at 269 and 336 nm for $[Rh(en)_2phi]^{3+}$, at 359 nm for $[Rh([12]aneN_4)phi]^{3+}$, and at 288, 306, and 364 nm for $[Rh([12]aneS_4)phi]^{3+}$, indicative of a clean deprotonation reaction. Taking the UV spectra in different organic solvents results in the same spectral changes as those seen in water at different pH. The spectroscopic changes are completely reversible over the pH range 2–11 for the complexes with aliphatic amine ligands. Irreversible changes in the spectrum of $[Rh([12]aneS_4)phi]^{3+}$ are observed at high pH (>10) due to decomposition. The pK_a for each complex may be obtained from the inflection point in plots of absorbance versus pH, and they are given in Table VI. As evident from the table, there is a strong inverse correlation between the acidity of the coordinated phi and the basicity of the ancillary ligands. As the base strength of the donor atoms of the ancillary ligands decreases in the order 4 NH_3, 2 en, $[12]aneN_4$ > 2 phen > [12]-

(35) Zefirov, N. S. *Tetrahedron* **1977**, *33*, 3193 and references cited therein.

Table VI. pH- and Structure-Dependent Electronic Transitions of Phi Complexes of Rhodium(III)

complex	ligand pK_b	complex pK_a	angle X_{ax}–Rh–X_{ax}	low-energy transition, nm: low pH	low-energy transition, nm: high pH
$[Rh(NH_3)_4phi]^{3+}$	4.75	9.2	179.3(1)	372, 386 (s)	364–373
$[Rh(en)_2phi]^{3+}$	3.3	9.1	176.0(6)	376, 389 (s)	363–375
α-$[Rh(Me_2trien)phi]^{3+}$ [a]	3–4	9.1	178.3(3)	373, 389 (s)	361–373
β-$[Rh(Me_2trien)phi]^{3+}$ [a]	3–4	8.9	166.1(2)	387	371–381
$[Rh([12]aneN_4)phi]^{3+}$	3–4	9.2	159.8(3)	395, 410 (s)	377–388
$[Rh(phen)_2phi]^{3+}$	9.2	6.2	168.8(1)[b]	380	358
$[Rh([12]aneS_4)phi]^{3+}$	≈19	4.7	168.5(1)	381	(327), 359
SiPhi				375	375

[a] Taken from ref 11. [b] $[Ru(bpy)_2phi](BF_4)_2 \cdot 0.19H_2O$ has been crystallized; this value is taken from ref 6.

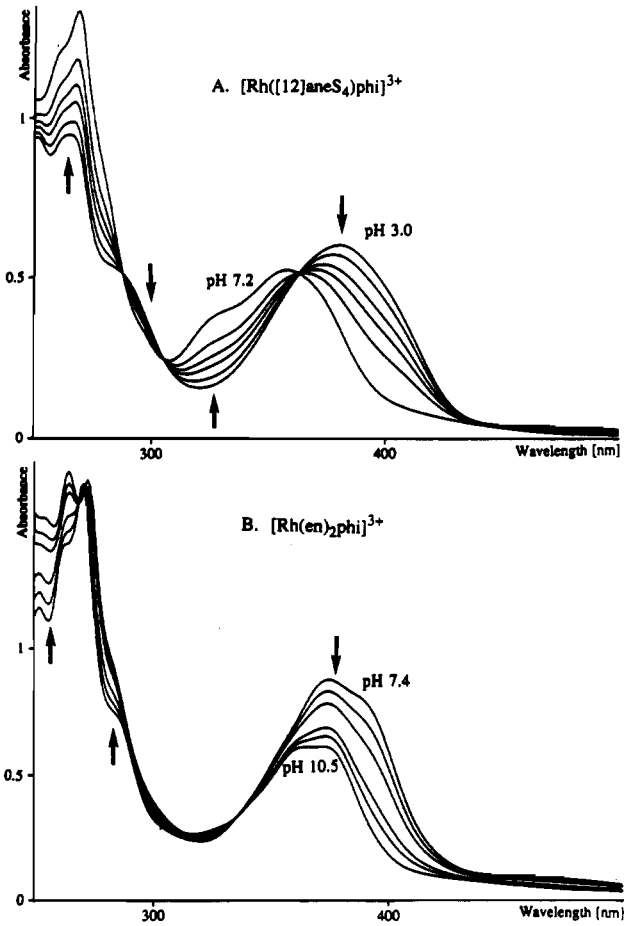

Figure 7. Electronic absorption spectra of $[Rh([12]aneS_4)phi]^{3+}$ (top) and $[Rh(en)_2phi]^{3+}$ (bottom) as a function of pH. Arrows indicate the starting spectrum at pH 3.0 and 7.4, respectively. Note the blue-shifts and the drop of intensity. Spectra taken at lower or higher pH than the lowest or highest pH shown do not show significant changes.

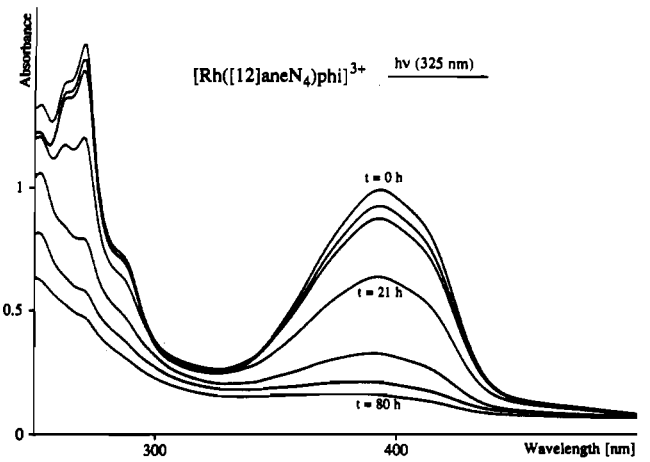

Figure 8. Photolysis of $[Rh([12]aneN_4)phi]^{3+}$ (two isomers) monitored by UV–visible spectroscopy showing the dissociation of the phi ligand.

$aneS_4$, the acidity of the phi imine hydrogen increases as reflected in the optical pK_a value.

The energy of the long-wavelength transition between 360 and 420 nm depends upon the coordination geometry of ancillary ligands of similar basicity. Increasing the distortion from octahedral geometry of the ancillary ligands in $[Rh(N_4)phi]^{3+}$ as seen in N_{ax}–Rh–N_{ax} angles, in the order NH_3, en_2, α-Me_2-trien[11] (N_{ax}–Rh–N_{ax} = 179.3(1), 176.0(6), 178.3(3)°) < β-Me_2-trien[11] (N_{ax}–Rh–N_{ax} = 166.1(2)°) < [12]aneN4 (N_{ax}–Rh–N_{ax} = 159.8(3)°), results in a substantial red-shift of the low-energy transition. While this observation does not establish the transition to be charge transfer in character, it suggests some mixing between the metal d-orbitals and the π-system of the phi ligand. This description is consistent also with optical studies of $[Rh(bpy)(2\text{-phenylpyridine})_2]PF_6$ in which comparable transitions are proposed to contain an admixture of $^1d\pi^*$ excitations.[36] A more detailed investigation of the origin of the photophysical features is currently in progress.

These spectra may also be compared to those of *N,N*-bis(trimethylsilyl)phenanthrenequinone diimine (SiPhi) and phi. For SiPhi, in heptane, two bands are detected in the same region as found with the rhodium complexes but with substantially lower intensity; at 360 nm, ϵ = 1700 M^{-1} cm^{-1}, and at 300 nm, ϵ = 4000 M^{-1} cm^{-1}. The low-energy band at 360 nm does not show solvent-dependent shifts when changing the solvent from low polarity (heptane, benzene) to high polarity (acetonitrile), as expected for π–π^* transitions. Spectra in protic solvents cannot be taken due to the instability of the silyl imine group. The spectrum of phenanthrenequinone diimine (phi) may also be obtained but also not in aqueous media. In heptane with 1% EtOH, absorption maxima for phi are at 367 nm, ϵ = 1500 M^{-1} cm^{-1}, and at 300 nm, ϵ = 2800 M^{-1} cm^{-1}. Comparing SiPhi and phi in the same solvent, then, one sees that the low-energy band is slightly shifted (~10 nm) to the red in the phi spectra, and phi shows a slight solvent-dependence. In contrast to SiPhi, free or coordinated phi can interact as a hydrogen-bond donor. The solvent dependence suggests that hydrogen bonding or dipole–dipole interactions between the solvent and the imine group affect the spectrum in the low-energy range. The bulky trimethylsilyl groups at the imine group also likely minimizes solvent effects at this polar group.

Photoreactivity of the Complexes. The 9,10-phenanthrenequinone diimine complexes of rhodium(III) $[Rh(phen)_2phi]^{3+}$ and $[Rh(phi)_2bpy]^{3+}$ undergo photoaquation upon irradiation with UV light at 313 or 325 nm. A mechanism of action has been proposed that involves an electron transfer from the phi ligand to the Rh(III) center with formation of a transient rhodium(II)phi-cation radical species $[Rh(II)^{2+}phi^{\bullet+}]$. The complexes described here show similar photoreactivity. Irradiation at ambient temperature with UV light at 325 nm with a He/Cd

(36) Frei, G.; Zilian, A.; Raselli, A.; Gudel, H. U.; Burgi, H. B. *Inorg. Chem.* **1992**, *31*, 4766–4773.

Table VII. Photochemical Parameters for Phi Complexes of Rhodium

complex	pK_a	pH	$10^{-3}\epsilon_{325\ nm}$, $M^{-1}\ cm^{-1}$	$10^4\Phi$[a]
$[Rh(NH_3)_4phi]^{3+}$	9.2	10	3.10	6.4(4)
		7	3.10	0.3(1)
$[Rh(en)_2phi]^{3+}$	9.1	10	3.40	10(1)
		7	3.30	0.3(1)
$[Rh([12]aneN_4)phi]^{3+}$	9.0	11	5.60	2.1(3)
		7	3.10	0.7(1)
$[Rh([12]aneS_4)phi]^{3+}$	4.7	7	10.50	2.1(3)
		2	5.40	0.4(1)
$[Rh(phen)_2phi]^{3+}$	6.2	7	13.90	5.2(5)
		2	10.20	0.04(1)

[a] Quantum yield for photodecomposition.

laser or at 313 nm with a Hg/Xe lamp leads to degradation of the $[Rh(X_4)phi]^{3+}$ complex within hours with preferential loss of the phi ligand, as indicated by UV/vis or ^1H NMR spectroscopy. No degradation occurs in the absence of light at ambient temperatures over several days. A representative spectrum of $[Rh([12]aneN_4)phi]^{3+}$ upon irradiation with a laser at 325 nm shows the loss of the absorption of the coordinated phi ligand (Figure 8), which provides evidence that photodecomposition involves dissociation of the phi ligand. The quantum yields as a function of pH are given for the photodissociation of $[Rh(NH_3)_4phi]^{3+}$, $[Rh(en)_2phi]^{3+}$, $[Rh([12]aneN_4)phi]^{3+}$, $[Rh([12]aneS_4)phi]^{3+}$, and $[Rh(phen)_2phi]^{3+}$ in Table VII.

Quantum yields depend very strongly on the protonation state of the phenanthrenequinone diimine ligand in the complexes. They are significantly lower at a pH below the pK_a of the complex than at a pH above the pK_a. Quantum yields at pH 7 for complexes $[Rh(NH_3)_4phi]^{3+}$ (pK_a 9.2), $[Rh(en)_2phi]^{3+}$ (pK_a 9.1), and $[Rh([12]aneN_4)phi]^{3+}$ (pK_a 9.0) range $(0.3–0.7) \times 10^{-4}$ and compare to the quantum yield of 0.4×10^{-4} of $[Rh([12]aneS_4]phi]^{3+}$ (pK_a 4.7) measured at pH 2. The quantum yield of 0.04×10^{-4} of $[Rh(phen)_2phi]^{3+}$ (pK_a 6.2) at pH 2 is about 1 order of magnitude lower. Raising the pH above the pK_a of the complexes increases the quantum yield, in same cases dramatically. The quantum yields of $[Rh(NH_3)_4phi]^{3+}$, $[Rh(en)_2phi]^{3+}$, and $[Rh([12]aneN_4)phi]^{3+}$, measured at pH 10 or 11, and of $[Rh([12]aneS_4]phi]^{3+}$ and $Rh(phen)_2phi]^{3+}$, measured at pH 7, range $(2–10) \times 10^{-4}$. These results support further our notion of a mechanism of photodecomposition, in which an electron transfer from the coordinated phenanthrenequinone diimine ligand to the rhodium(III) center is involved.

Acknowledgment. We are grateful to the National Institutes of Health (Grant GM33309) for their financial support, and A.H.K. thanks the Deutsche Forschungsgemeinschaft for a postdoctoral fellowship. We are also grateful to W. P. Schaefer for carrying out the crystallographic studies in the Beckman Institute.

Supplementary Material Available: Tables of final heavy-atom parameters, assigned hydrogen atom parameters, anisotropic displacement parameters, complete distances and angles, and interionic and intermolecular distances less than 3.5 Å for $[Rh(NH_3)_4phi]Cl_3 \cdot 3H_2O$ (Tables S1–S5), $[Rh([12]aneN_4)phi](SCN)_3 \cdot 2H_2O$ (Table S6–S10), and $[Rh([12]aneS_4)phi]Br_3 \cdot 3H_2O$ (Tables S11–S15), distances of atoms of ancillary ligands in $[Rh(NH_3)_4phi]^{3+}$, $[Rh(en)_2phi]^{3+}$, $[Rh([12]aneN_4)phi]^{3+}$, and $[Rh([12]aneS_4)phi]^{3+}$ to planes A, B, and C (Table S16), and UV–visible data Table S17) and figures showing the contents of a unit cell of $[Rh([12]aneN_4)phi](SCN)_3 \cdot 2H_2O$ (Figure S1) and $[Rh([12]aneS_4)phi]Br_3 \cdot 3H_2O$ (Figure S2) together with a view perpendicular to the aromatic ligand and a ^{13}C NMR spectrum of a mixture of C_s- and C_{2v}-$[Rh([12]aneN_4)phi]^{3+}$ including a HPL-chromatogram (Figure S3) (37 pages). Ordering information is given on any current masthead page.